The cloud radiative effects of International Satellite Cloud Climatology Project weather states

Lazaros Oreopoulos[1] and William. B. Rossow[2]

Received 9 December 2010; revised 28 February 2011; accepted 26 March 2011; published 17 June 2011.

[1] The salient features of the daytime cloud radiative effect (CRE, also known as cloud radiative forcing) corresponding to various cloud regimes or weather states are examined. The analysis is based on a 24 year long data set from the International Satellite Cloud Climatology Project (ISCCP) for three distinct geographical zones covering most of the Earth's surface area. Conditional sampling and averaging of the ISCCP cloud fraction and CRE in 2.5° grid cells is performed for each weather state, and the state's radiative importance expressed as the relative contribution to the total CRE of its geographical zone is explained in terms of dominant cloud type, cloud fraction, and frequency of occurrence. Similarities and differences within and between geographical zones in the cloud fraction and CRE characteristics of the various weather states are identified and highlighted. By providing an exposition of the radiative energy characteristics of different cloud type mixtures, we facilitate the meteorological situation-dependent evaluation of radiation budget effects due to clouds in climate models.

Citation: Oreopoulos, L., and W. B. Rossow (2011), The cloud radiative effects of International Satellite Cloud Climatology Project weather states, *J. Geophys. Res.*, *116*, D12202, doi:10.1029/2010JD015472.

1. Introduction

[2] Attribution of cloud contributions to Earth's radiation budget in both observations and General Circulation Models (GCMs) have generally been limited to ensemble averages of the difference between radiative fluxes for clear and cloudy skies, referred to as either the cloud radiative forcing [*Ramanathan et al.*, 1989] or the cloud radiative effect (CRE) [e.g., *Rossow and Lacis*, 1990; *Zhang et al.*, 1995, 2004; *Pincus et al.*, 2008]. This "bulk" approach provides only a first-order estimate of the overall radiative effects of clouds, but has nonetheless been used as the primary way to compare GCMs to observations. Direct determinations of radiative fluxes from measured cloud properties [*Rossow and Lacis*, 1990; *Zhang et al.*, 1995; *Rossow and Zhang*, 1995; *Zhang et al.*, 2004] provide a more diagnostic alternative because results can be sorted by specific cloud types (see *Zhang et al.* [1995] for discussion of older studies). In general, however, efforts to quantify CRE by cloud type have been only sporadic [*Hartmann et al.*, 1992; *Rossow and Zhang*, 1995; *Chen et al.*, 2000; *Webb et al.*, 2001]. The recent GCM evaluation study by *Williams and Webb* [2009] illustrates how such a diagnostic analysis of clouds and radiation budgets can provide better insight into simulated cloud regimes and their associated radiative effects.

[3] Satellite retrievals of cloud properties allow for similar analyses using a systematic classification of "cloud types" [cf. *Rossow and Schiffer*, 1991; *Lau and Crane*, 1995; *Hahn et al.*, 2001], but other approaches are possible such as recent efforts to define meteorologically relevant "cloud regimes" or "weather states" via cluster analysis of cloud top pressure–optical thickness covariations at the mesoscale [*Jakob and Tselioudis*, 2003; *Jakob et al.*, 2005; *Rossow et al.*, 2005]. Associating such mesoscale cloud property classifications with differing meteorology allows connecting their radiation budget effects to dynamical processes for better insight and the ability to evaluate the quality of GCM representations in terms of the impact of the dynamics-cloud-radiation interactions on other aspects of a GCM's climate [*Williams and Tselioudis*, 2007; *Williams and Webb*, 2009]. This is both a more informative and more challenging way to evaluate GCM cloud process simulations since cloud properties and radiative effects are related more directly and objectively to the meteorological situation. Caution is required, however, in interpreting such statistical classification results, like those from the clustering method, because they can depend on the domain and data set size [cf. *Chéruy and Aires*, 2009]. More importantly, the classification depends on the variables selected to define the "classification space" [cf. *Rossow et al.*, 2005; *Gordon et al.*, 2005; *Chen and Del Genio*, 2009; *Zhang et al.*, 2007, 2010; *Greenwald et al.*, 2010], an issue that deserves more investigation. Here we use the "cloud regimes," which we will henceforth call "weather states" as by *Rossow et al.* [2005], that are based on 24 years of mesoscale joint histograms of cloud top pressure–optical thickness from the International Satellite Cloud Climatology Project (ISCCP) [*Schiffer and Rossow*, 1983].

[1]Laboratory for Atmospheres, NASA Goddard Space Flight Center, Greenbelt, Maryland, USA.
[2]NOAA Cooperative Remote Sensing Science and Technology Center, City College of New York, New York, New York, USA.

Copyright 2011 by the American Geophysical Union.
0148-0227/11/2010JD015472

[4] *Rossow and Schiffer* [1991] first suggested that the covariation of cloud top pressure–optical thickness exhibited distinctive patterns in the well-known climatological regimes. *Lau and Crane* [1995] showed that the ISCCP cloud types, based on the joint values of cloud top pressure and optical thickness, correspond to the classical morphological cloud types within tropical and midlatitude storms. *Hahn et al.* [2001] went further and showed that the correspondence between the surface observer's classical cloud morphological types and that seen by satellite (ISCCP) was stronger when the latter was represented by distinctive mesoscale patterns in the cloud properties. *Jakob and Tselioudis* [2003], *Jakob et al.* [2005], *Tromeur and Rossow* [2010], *Mekonnen and Rossow* [2011], and *Tselioudis and Rossow* [2011] have all shown evidence linking the ISCCP cloud regimes in the tropics to distinct atmospheric conditions. Recently *Haynes et al.* [2011] has presented similar evidence for midlatitude cyclones in the southern hemisphere.

[5] For the purpose of climate model evaluation, the assumptions and criteria of such procedures are not of critical importance as long as the same assumptions and criteria are also applied to the model output. With the use of satellite simulators becoming more common in models, particularly the ISCCP Simulator [*Klein and Jakob*, 1999], this type of analysis is now more readily possible. However, studies that establish relationships between clouds, radiation and the atmospheric circulation will be even more valuable for evaluating the quality of cloud radiation process representation in climate models.

[6] Our study provides an example of how satellite retrievals of cloud properties and the associated radiation budget data can be used to better diagnose these relationships. We quantify the CRE (from the ISCCP FD product [*Zhang et al.*, 2004]) associated with each ISCCP [*Rossow and Schiffer*, 1999] weather state (ISCCP D1.WS product, http://isccp.giss.nasa.gov/climanal5.html) between 65°S and 65°N by conditional sorting and averaging. Note that while the ISCCP FD product is based on calculations of the specific effects of the ISCCP cloud types identified by their optical thickness and top pressure, the weather state analysis identifies distinct mesoscale *mixtures* of cloud types so that our conditional sorting will reveal novel relationships. We identify the radiatively most important weather states as determined by their relative frequency of occurrence (RFO), their cloud fraction (CF) and their CRE at the time of occurrence. Such information has obvious use for studying GCM skill in simulating regional and global radiative balance without compensating errors.

2. The ISCCP Weather States

[7] *Rossow et al.* [2005] searched for distinctive patterns in the joint frequency distributions of cloud top pressure (p_c) and cloud optical thickness (τ) constructed from individual satellite image pixel retrievals (fields of view about 5 km in size) within 2.5° regions that are provided in the International Satellite Cloud Climatology (ISCCP) D1 data set [*Rossow and Schiffer*, 1999]. Their results were limited to the tropical regions (±15° latitude) and covered 21.5 years (mid-1983 to 2004). Cluster centroids representing specific histogram patterns describing cloud variability were identified using the "K-means" clustering algorithm [*Anderberg*, 1973] applied to 3-hourly p_c-τ histograms of 2.5° regions, including completely clear regions. Through an iterative procedure, each p_c-τ histogram for each 3 h time interval in each 2.5° map grid cell in this tropical zone was assigned to one of 6 clusters based on an Euclidean distance minimization metric. The criteria for deciding on the optimum number of clusters consisted of checks that the results were statistically robust (trials with many initial seeds, comparisons of results from data record subsets), that the ratio of cluster population dispersion to centroid separation distance was less than 0.5, that the cluster centroid patterns did not correlate, and that the cluster RFOs had different geographic distributions [*Rossow et al.*, 2005]. We follow *Rossow et al.* [2005] and refer to these cloud property patterns as "weather states" (WS) with the understanding that they represent cloud type mixtures or "cloud regimes" that have been shown to be associated with distinct atmospheric conditions [*Jakob and Tselioudis*, 2003; *Jakob et al.*, 2005; *Gordon and Norris*, 2010]. That particular cloud regimes are associated with particular synoptic conditions was also demonstrated by *Marchand et al.* [2009], who showed that clustering synoptic atmospheric conditions yields distinct patterns of hydrometeor occurrence.

[8] Recently ISCCP has extended the cluster analysis previously described to additional years and geographic regions (the relevant data can be downloaded from ftp://isccp.giss.nasa.gov/outgoing/PICKUP/CLUSTERS/data/1983–2008/). The joint histograms of the 2.5° cells were assigned to weather states identified with the above algorithm by performing a separate analysis for the extended tropical/subtropical zone (35°S to 35°N, ISCCP data set D1.WS.ET.dat, we often refer to this zone simply as "tropical" or "the tropics") – a data set that has been used by *Mekonnen and Rossow* [2011], the northern midlatitudes (35°N to 65°N, ISCCP data set D1.WS.MN.dat), and the southern midlatitudes (35°S to 65°S, ISCCP data set D1.WS.MS.dat) – a data set that has been used by *Haynes et al.* [2011]. The optimal centroids for these geographical regions are shown in Figures 1, 7, and 13, while maps of their RFO are provided in Figures 2, 8, and 14. Weather state indices for these other regions are assigned according to the convention by *Rossow et al.* [2005], i.e., they increase as the states become more convectively suppressed or contain fewer precipitating clouds.

[9] Many of the centroids of the current tropical data set correspond to cloud patterns similar to those in the narrower tropical zone by *Rossow et al.* [2005]. This is not unexpected for the current extended tropics region, but holds true to some extent for the midlatitude regions as well. The reason is that the centroids must reflect to some degree common mixtures of cloud types encountered in all climatic zones and identified by standard cloud classification methods. For example, WS4 of the tropical zone which is dominated by high thin cirrus clouds has counterparts in both the northern and southern midlatitude zones (WS5 in both cases). Other correspondences that can be immediately identified are tropical WS5 representing a similar cloud mixture as northern midlatitude WS7 and southern midlatitude WS6 (dominated by stratus/stratocumulus); WS2 in all geographical zones containing high numbers of mesoscale anvil and congestus-like clouds. On the other hand, there exist weather states in one region that do not have counterparts in the other regions, for example midlatitude WS3 (both northern and southern)

apparently containing many storm-track clouds (e.g., nimbostratus) that are virtually absent from the tropics (as noted by *Warren et al.* [1986, 1988]). Even in midlatitudes the correspondence between weather states is imperfect; for example the north has two weather states dominated by high thin clouds (WS5 and WS6), while the south has only one, but the second northern weather state (WS6) apparently represents cloud regimes where overlap with lower clouds is distinct and frequent enough to justify a separate weather state. This difference arises because of the differing amounts of land in the two hemispheres as seen in Figure 8 where northern midlatitude WS6 appears frequently over land regions.

3. Data and Analysis Method

[10] We use 24 years of ISCCP weather state and radiative flux data (1984–2007). The analysis approach is fairly straightforward. The D1.WS.ET.dat, D1.WS.MN.dat, and D1.WS.MS.dat files contain the weather state in each 2.5° grid cell as an integer that ranges from 0 to 9 (0 corresponds to clear skies; in the northern midlatitudes the index can be as high as 9) for every daily 3 h interval. Weather states are assigned to only sunlit grid cells, otherwise the data point is designated as missing. ISCCP FD data [*Zhang et al.*, 2004] provide clear and overcast-sky radiative flux and total cloud fraction (CF) data for the same period at identical temporal and spatial resolution. The fluxes are derived using a broadband radiative transfer code into which ISCCP retrievals of cloud properties and surface albedo, as well as other ancillary atmospheric and surface information, are passed (for details, see *Zhang et al.* [2004]). The Cloud Radiative Effect CRE is calculated as:

$$CRE^{\mathrm{TOA/SFC}}_{\mathrm{SW/LW/NET}} = CF\left[F^{\mathrm{TOA/SFC}}_{\mathrm{SW/LW/NET}}(clr) - F^{\mathrm{TOA/SFC}}_{\mathrm{SW/LW/NET}}(ovc)\right] \quad (1)$$

i.e., the difference between clear (clr) and overcast (ovc) shortwave (SW), longwave (LW) and net (SW + LW) fluxes (F) at the top of the atmosphere (TOA) or the surface (SFC) multiplied by CF. The flux is defined as positive upward at the TOA and downward at the surface. With this CRE definition and sign convention, TOA SW CRE is usually negative and SFC SW CRE is usually positive, i.e., adding clouds cools the planet, primarily the surface. TOA LW CRE is usually positive and SFC LW CRE is usually negative, i.e., adding clouds heats the planet, primarily the atmosphere. Net (= SW + LW) CREs at TOA and SFC can be either positive or negative. Note that $F(ovc)$ is determined in ISCCP FD by dividing the "all-sky" flux values by CF, where "all-sky" flux values are determined by the actual fractional amounts of the radiative cloud types defined by optical thickness and cloud top pressure as well as a climatology of cloud vertical structure [*Zhang et al.*, 2004]. Also note that this method of calculating CRE differs from its more direct determination from broadband satellite fluxes where cloudy sky fluxes are subtracted from their separately aggregated clear-sky counterparts. In the ISCCP FD method of calculating CRE, an estimate is possible even when conditions are perpetually overcast: to perform the clear-sky flux calculation one simply removes the cloud from the radiative transfer model, leaving everything else unchanged.

[11] For each 2.5° grid cell and 3 h time period, we segregate the CF and CRE values that correspond to a particular weather state. From the segregated data set we then calculate monthly means of the area-averaged daytime CF and CRE for each weather state, *when present*, within each geographical zone for the entire 24 year period, as well as their percentage contributions to the total CF and CRE. We also calculate the frequency distributions of SW, LW and net CRE of each weather state for the entire data set period. These contain information on the spatial and temporal mesoscale variations of a state's CRE. We must emphasize that no radiative flux calculations were performed specifically for this study. We simply performed conditional sampling and averaging of already available ISCCP FD fluxes for each spatially and temporally coincident weather state.

[12] We present results mostly for TOA CREs which seem sufficient for characterizing the radiative importance and distinctiveness of each weather state, especially in the SW. In the LW, the absolute values of TOA and SFC CRE can be quite different and when examined together can add further insight into the nature of the weather states and their link to dynamical processes and the surrounding environment. LW CRE comparisons between TOA and SFC are therefore included in the presentation that follows.

4. Weather State Radiative Effects

[13] Sections 4.1–4.3 are devoted to the analysis of a single geographical zone. They follow a similar narrative that includes a discussion of weather state groupings based on their annually averaged daytime cloud fractions (when present) and occurrence frequencies, the values of the mean daytime SW, LW (TOA and SFC), and net CRE, as well as the percent contribution to the total cloud fraction and CRE of each weather state. We also present the CRE frequency distributions which characterize spatial and temporal (i.e., synoptic) CRE variability. Our analysis intends to shed light on: (1) the weather state mean annual CF and CRE at the time of occurrence and the range of seasonal variations; (2) the relative importance of each weather state in terms of contribution to the total CRE within its geographical zone; and (3) the degree of radiative distinctiveness of weather states according to CRE.

4.1. Extended Tropics

[14] The ISCCP WS centroids for the extended tropics are shown in Figure 1, while the geographic distribution of their annually averaged RFO is depicted in Figure 2. Besides RFO, a weather state property with critical role in its ultimate radiative importance is the mean CF at the time of occurrence since a frequently occurring state has significant radiative impact only with corresponding high CFs. Figure 3 shows the RFOs, annually averaged CFs when present, and percent contributions to the total CFs of each weather state in the tropics. The error bars superimposed on each column bar are the standard deviations (sdev) of the twelve monthly means of the corresponding quantities, i.e., they represent seasonal variability.

[15] WS1 and WS2 (with a prevalence of high clouds of medium to large optical thickness, including thick cirrus anvils), represent cloud regimes that are nearly overcast at

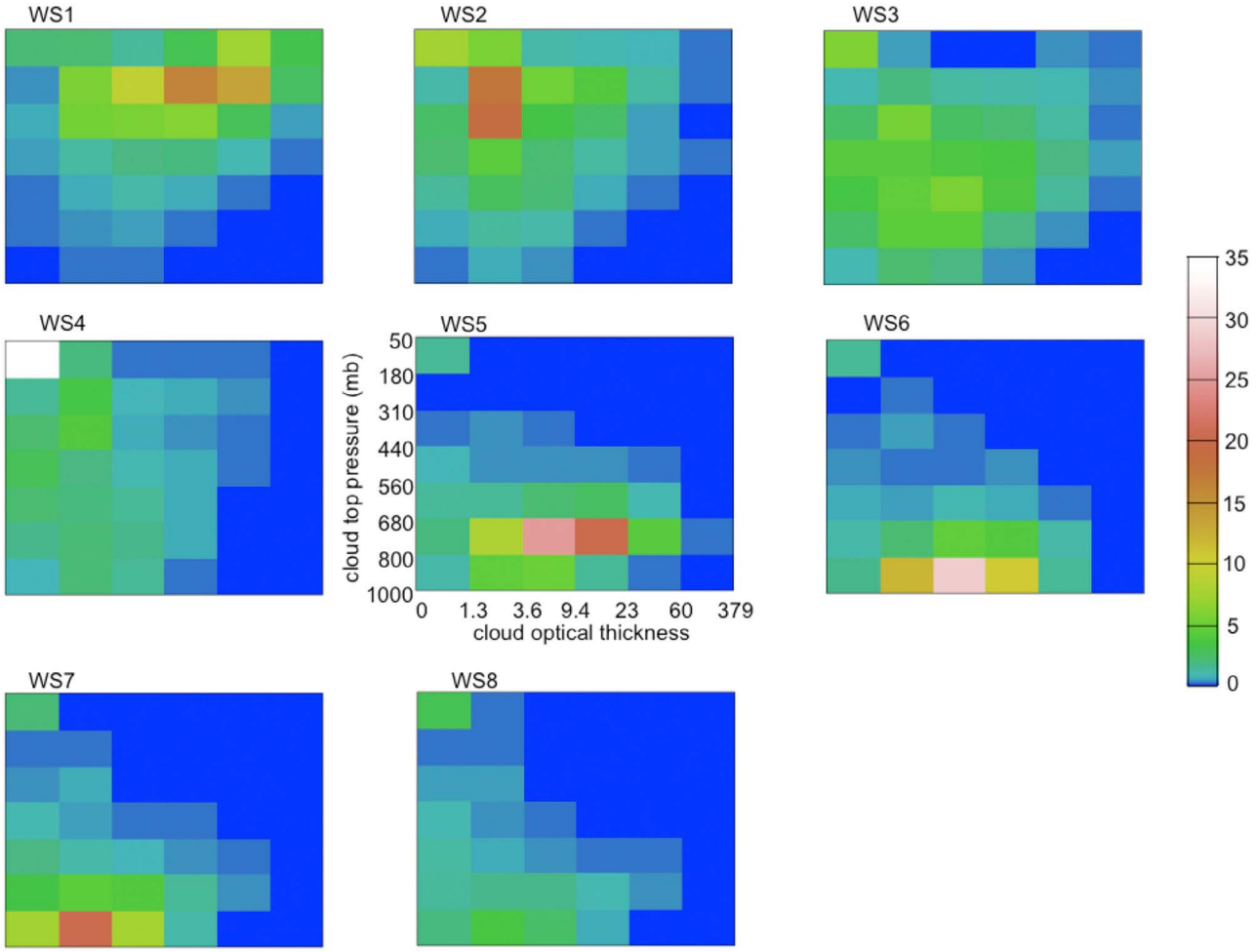

Figure 1. The cluster centroids of the eight weather states of the extended tropics geographical zone (35°S to 35°N) derived from ISCCP. Each plot shows the normalized frequency of occurrence (in %) within p_c-τ bins.

the mesoscale when they occur, while WS3, WS4, WS5, and WS6, which correspond to quite disparate cloud regimes (see Figure 1), all have annually averaged CFs above 0.7 (WS3 and WS5 have the largest CFs within this group). WS7 (dominated by broken stratocumulus/trade cumulus) is distinct with an annual CF of ~0.6, while the lowest CF by far belongs to WS8 (a mixture of fair weather cumulus with some overlying high thin cloud). The minute error bars clearly indicate that the annual cycle of CF is very weak for all weather states, consistent with the weak meteorological seasonality in the tropics and the fact that this zone is symmetric about the equator. A state's percent contribution to the total CF depends both on its CF when present and its RFO. The largest contributor to total CF is WS3 (primarily unorganized convection) with a large CF of ~0.8 and the second largest RFO of about 0.17. The smallest contribution does not come from the state with the smallest CF, WS8 (a mixture of trade cumulus and upper level clouds), but from the state with the smallest RFO, WS6 (dominated by marine and continental boundary layer clouds), despite the substantial mean CF when present of above 0.7. The state with the largest RFO (about double of the 2nd largest), WS8, is second in CF contribution. Seasonal variations in the contribution to the total CF are more notable for WS5 (containing large amounts of marine stratocumulus), which exhibits seasonal changes not so much in CF, but in RFO (it has the largest RFO sdev), followed closely by WS6. These variations represent more a seasonal variation of the cloud types from more overcast to more broken which can reallocate cloud mixtures to different weather states. The peak RFO for WS5 is encountered in August–September and the minimum in March–April (not shown); WS6 is slightly different in that the peak frequency occurs in July–August, while in September the frequency of occurrence drops to values close to the annual mean (not shown). These seasonal variations are consistent with the known annual cycle of marine stratus clouds [e.g., *Klein and Hartmann*, 1993; *Oreopoulos and Davies*, 1993] which seem to be major contributors to these weather states. At the opposite end, the states with the smallest RFO annual cycle are WS3 and WS8, followed closely by WS1. These three states correspond to rather different cloud regimes, but share the common trait that for no month is the RFO different from its annual mean by more than 5%.

[16] At the time of occurrence, the CRE of a WS depends on the CF and the two main factors that determine the

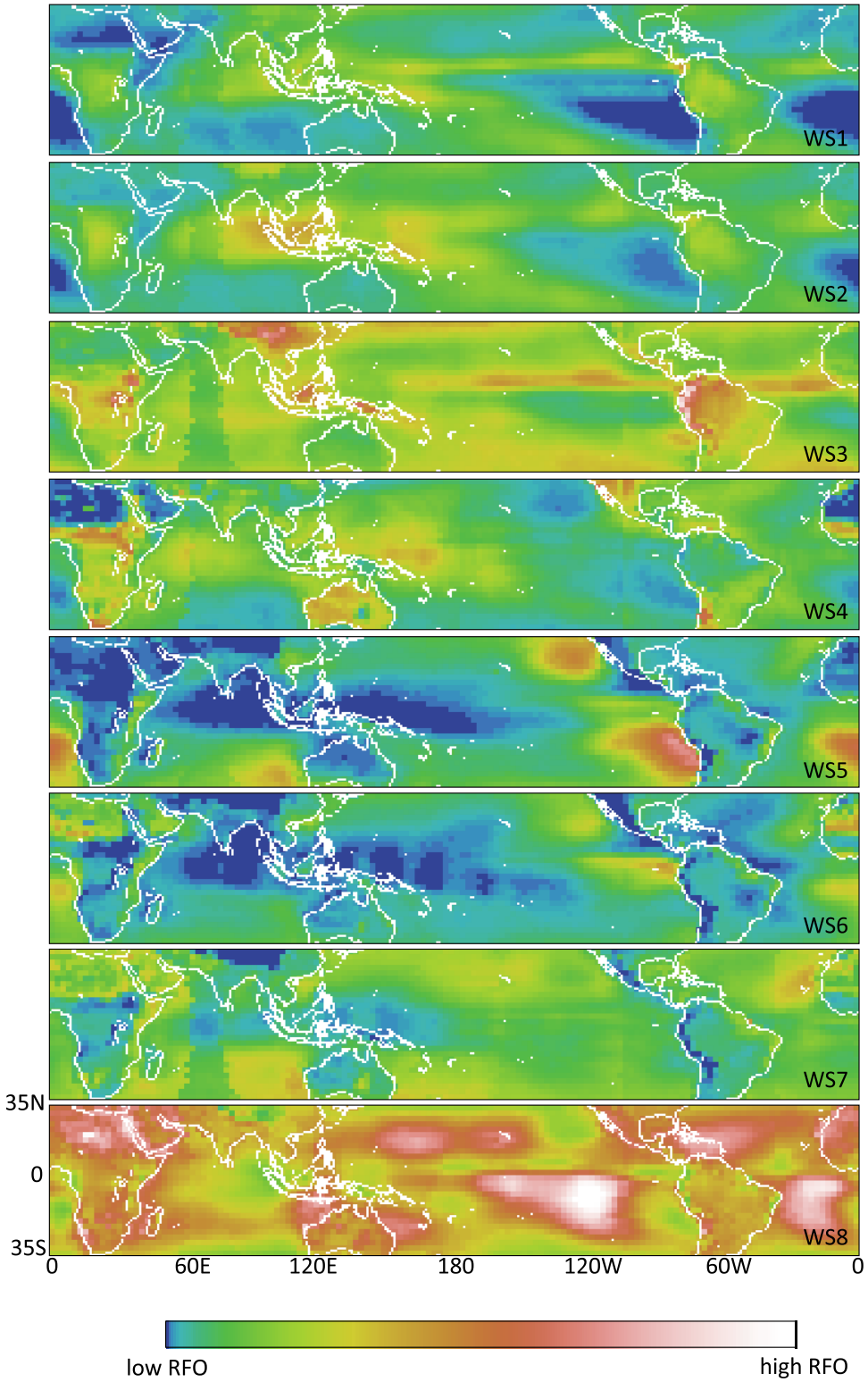

Figure 2. The geographic distribution of the relative frequency of occurrence (RFO) of the eight weather states of the extended tropics geographical zone for the period 1984–2007. Values are normalized relative to the total number of weather state occurrences for this period within the geographical area.

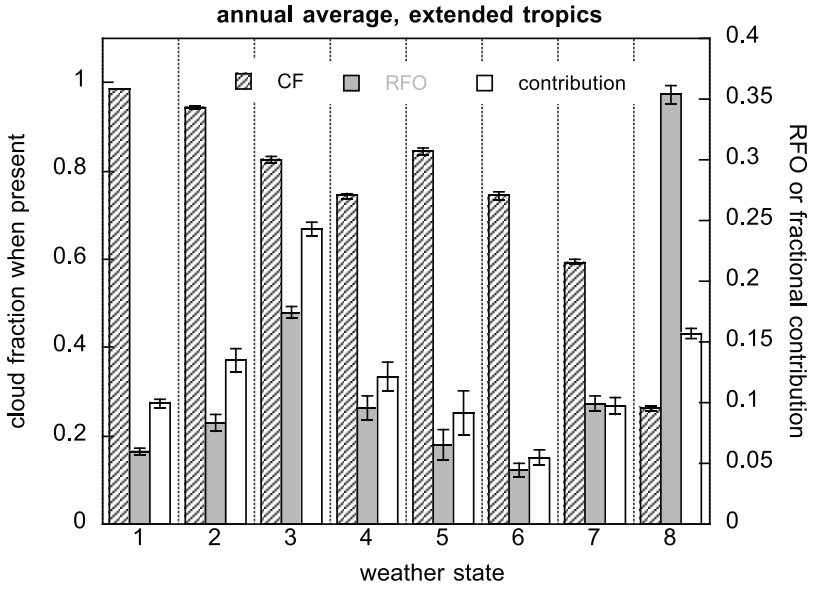

Figure 3. Relative frequency of occurrence (RFO), annually and spatially averaged cloud fraction (CF) when present, and fractional contribution to the total cloud fraction for each weather state of the extended tropics. The clear-sky (WS0) RFO is 0.025. The error bars are the standard deviations of the multiyear monthly means; that is, they are indicative of the seasonal variability of the domain-averaged quantities.

radiative flux of overcast skies in equation (1), namely, τ (mainly for SW), and the cloud vertical location (mainly for LW). Everything else being equal, the optically thicker the cloud, the greater its SW TOA and SFC CRE, and the higher the cloud top and the lower its base, the greater its LW TOA and SFC (respectively) CRE for a particular τ. Seasonal variations of SW CRE also depend of course on the amount of available solar insolation, and LW CRE seasonal changes are affected by seasonal changes in atmospheric temperatures and water vapor. In calculations of weather state *contributions* to the overall CRE, the RFO is obviously also a critical factor. With the above in mind, a basis for interpreting CRE behavior in all geographical zones is available.

[17] The CRE characteristics of the tropical weather states are summarized in Figures 4–6. Figure 4 (top) shows that annually averaged TOA LW CREs below 20 Wm^{-2} characterize WS5, WS6, WS7, WS8 (the least convectively active states), but the SW CREs assume a wide range (as do the net CREs) of values between -35 Wm^{-2} and -195 Wm^{-2} that correlate well with the dominant τ within these states shown in Figure 1. WS3 and WS4 are almost indistinguishable in terms of their average LW CRE, but separate very clearly in terms of SW (and net) CRE, both being larger for WS3, the more convectively active state of the two. WS1 and WS2 appear quite apart in LW-SW CRE space not just from the other weather states, but also from each other (their net CRE differs by ~150 Wm^{-2}). In addition to having the strongest LW CRE, WS1 also has the strongest SW CRE and net CRE. In contrast, WS8 has the weakest SW, LW and net CREs. WS4 and WS7 representing completely different cloud mixtures have almost indistinguishable SW CREs, but differ in net CRE because of their LW CRE differences. The greatest similarity in net CRE is between WS4 and WS8, even though they correspond to entirely different cloud mixtures with distinct LW and SW CRE components. Seasonal variations of LW CRE are very weak for all weather states (the maximum sdev of ~9% of the annual mean occurs for WS6). For the tropics, even the SW CRE cycle is rather weak (~8%, also for WS6). A notable feature of Figure 4 (top) is that only two states approach a nearly zero daytime TOA net CRE, one being the boundary layer cumulus-dominated WS8 and the other being the cirrus-dominated WS4, contradicting some claims that tropical deep convection produces this condition.

[18] In terms of contribution to the tropical TOA CRE (Figure 4, bottom) we observe the following: The states with the greatest mean LW CRE when present, WS1 and WS2, are two of the strongest contributors to the total LW CRE, but they are surpassed in contribution by WS3 which has a far larger RFO (see Figure 3). The top SW CRE contributor is again WS3, followed by WS1. WS3 achieves this because of its large RFO, while WS1 because of its large CF (Figure 3) and larger CRE when present (due to optically thicker clouds; see Figure 1). Despite the attention given to marine stratus as causing differences of climate model CRE, the weather states where they are prevalent are not the largest contributors to tropical and subtropical CRE; as Figure 4 shows, it is the convectively active states that contribute most of the SW CRE. WS1 and WS3 also stand out in terms of net daytime TOA CRE contributions. A second group of states (WS2, WS5 and WS8) has significant net CRE contributions as well, ranging from ~10 to ~14%. WS6 is one of the weakest contributors in all components of CRE, probably because of its low RFO, but WS4 (with many thin cirrus) is the weakest contributor to the overall net TOA CRE. The most seasonally varying contribution to CRE comes from WS5 which exhibits a sdev close to 20% of the mean for all

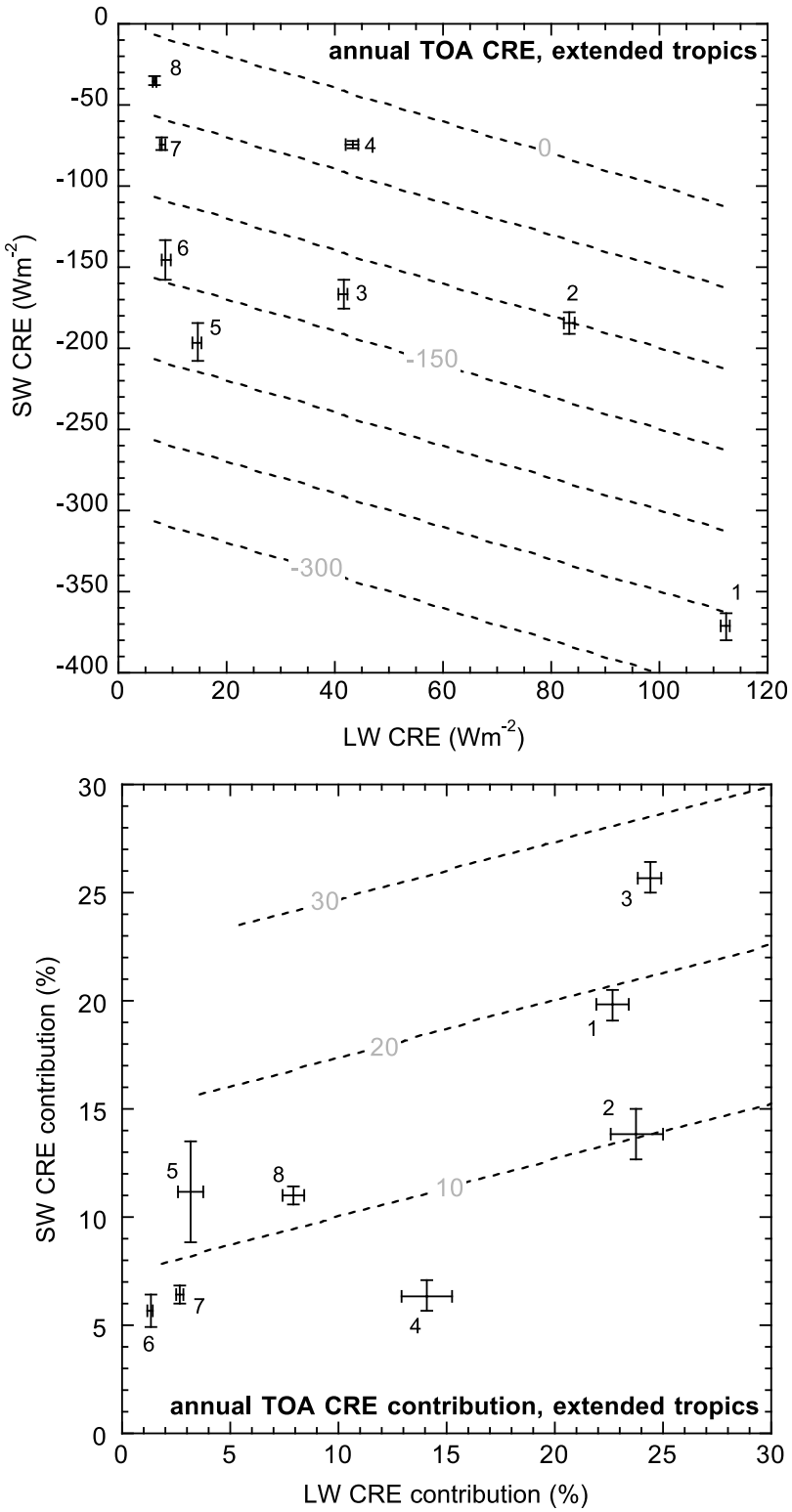

Figure 4. (top) Annually and spatially averaged daytime SW TOA CRE against its LW counterpart each weather state for the extended tropics. The dashed lines are lines of constant net CRE in increments of −50 Wm^{-2}, while the error bars are standard deviations of domain-averaged LW (horizontal bars) and SW (vertical bars) multiyear monthly CREs. (bottom) Same as Figure 4 (top) but for % CRE contributions of each weather state to the total CRE of the extended tropics. The dashed lines are lines of constant net % CRE contributions. The average SW and LW CRE values (or % contributions) occur at the intersection of the error bars.

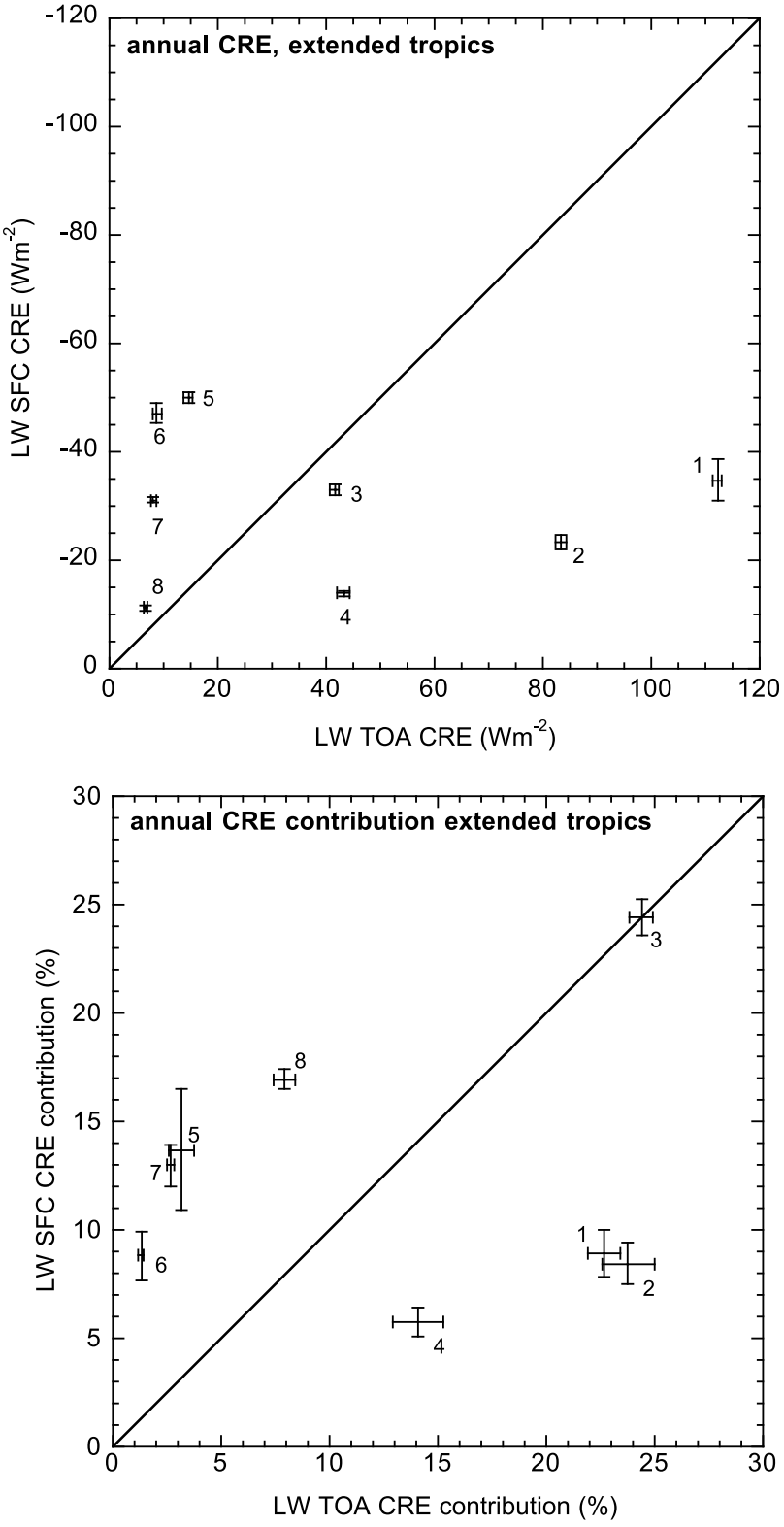

Figure 5. (top) Annually and spatially averaged daytime LW SFC CRE against its TOA counterpart for each weather state of the extended tropics. (bottom) Same as Figure 5 (top) but for % contributions. The average LW CRE values (or % contributions) occur at the intersection of the error bars.

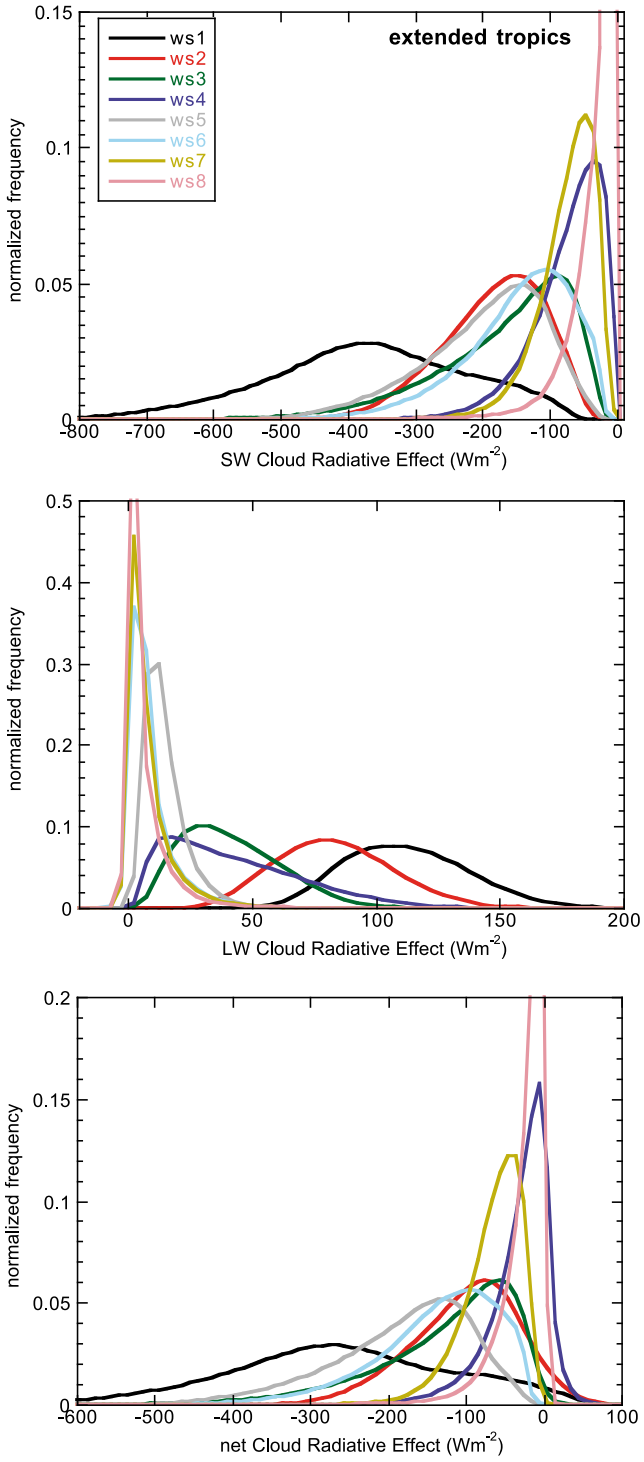

Figure 6. Normalized frequency distributions per weather state of each TOA CRE component for the extended tropics during the period 1984–2007. (top) SW CRE, (middle) LW CRE, and (bottom) net CRE.

three CRE components. We have previously seen that this weather state also stood out for its seasonal variability of CF contribution because of significant RFO seasonal variations.

[19] Figure 5 compares the LW CRE at TOA and SFC for the tropical region, the sum of which is indicative of the radiative heating of the atmosphere by clouds: weather states falling above the 1-to-1 line indicate cloud regimes cooling the atmosphere whereas states below the line indicate regimes warming the atmosphere. Although WS3 plays a major role in the TOA CRE, its net effect on LW heating of the atmosphere is nearly zero as is the contribution from the cloud regime with lots of scattered cumulus (WS8). The two stronger convective states, WS1 and WS2, produce a large heating of the tropical atmosphere, whereas all the boundary layer weather states (except WS8) produce a weaker cooling. Although the magnitude of the effect of WS4 is smaller than for the convective systems, its percentage contribution is substantial because of its somewhat larger RFO. These results reflect the general situation in low latitudes where the fair weather atmosphere is cooled by radiation and the surface is heated, even with some clouds present, but the CRE reinforces storm system latent heating of the atmosphere while cooling the surface.

[20] Histograms of TOA CRE components, shown in Figure 6 illuminate the synoptic variability and radiative similarities and differences among the weather states. For example, we compare the CRE histograms of states with similar mean CREs. LW mean CREs were most similar for WS3 and WS4, but the LW CRE histograms for these states are clearly distinct. The most similar mean SW CREs were for WS4 and WS7; their SW CRE histograms are also similar, but the WS4 is wider with more occurrences of both smaller and larger values of CRE. Something analogous can be seen in the histograms of WS4 and WS8 net CRE, which were the two states with closest mean values. The histograms of CRE also indicate the range of possible CRE values assumed by a particular weather state. WS1, the most convectively active state, has by far the widest histograms in all components of CRE (the other convectively active states also have quite wide LW CRE histograms), and in that sense cannot be assigned "typical" CRE values. On the other hand, the least convectively active states have quite narrow LW CRE histograms, but only for WS8 do the histograms for both other components remain narrow as well. The modal values of all three CRE component histograms can thus be considered representative CRE values for this particular state.

4.2. Northern Midlatitudes

[21] The ISCCP weather state centroids for the northern midlatitudes are shown in Figure 7, while the geographic distribution of their frequency of occurrence is shown in Figure 8. For this geographical zone six weather states (WS1, WS2, WS3, WS4, WS7, WS8) are characterized by mean total cloud fractions when present greater than 0.85 (Figure 9). A second group with quite large CFs (0.7–0.8) at 2.5° scales is formed by states WS5 and WS9 (dominated by thin cirrus and optically thin boundary layer clouds, respectively). The most frequently occurring state, WS6 (including multilayer clouds but with a predominance of boundary cumulus), is concentrated over land areas (and at the equatorward edge of the zone in the eastern Mediterranean) and is completely distinct from the other weather states in terms of CF, with mean values fluctuating between 0.4 and 0.5 throughout the year (highest in May, lowest in September–not shown). Moreover, WS6 exhibits

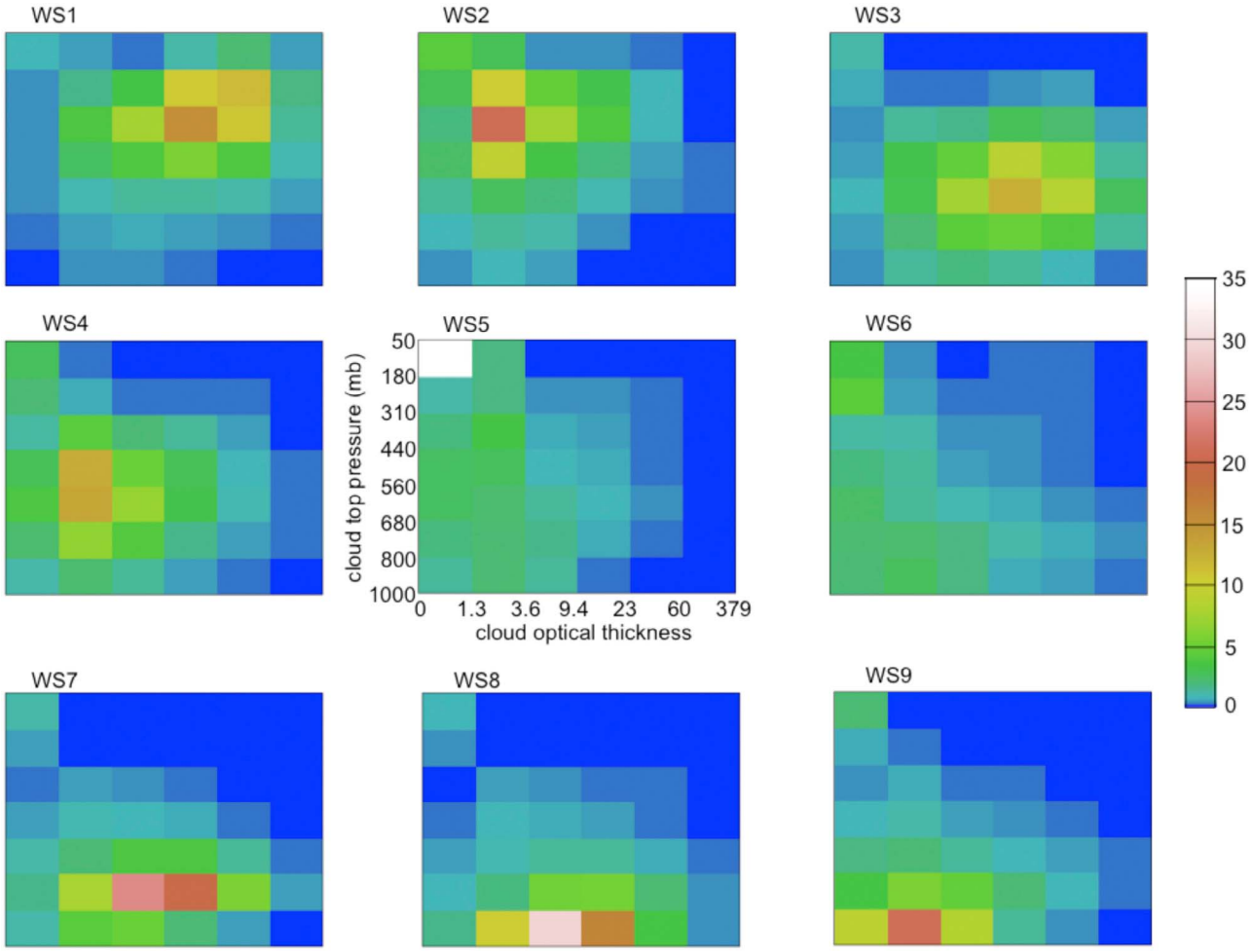

Figure 7. Same as Figure 1 but for the nine weather states of the northern midlatitudes (35°N to 65°N).

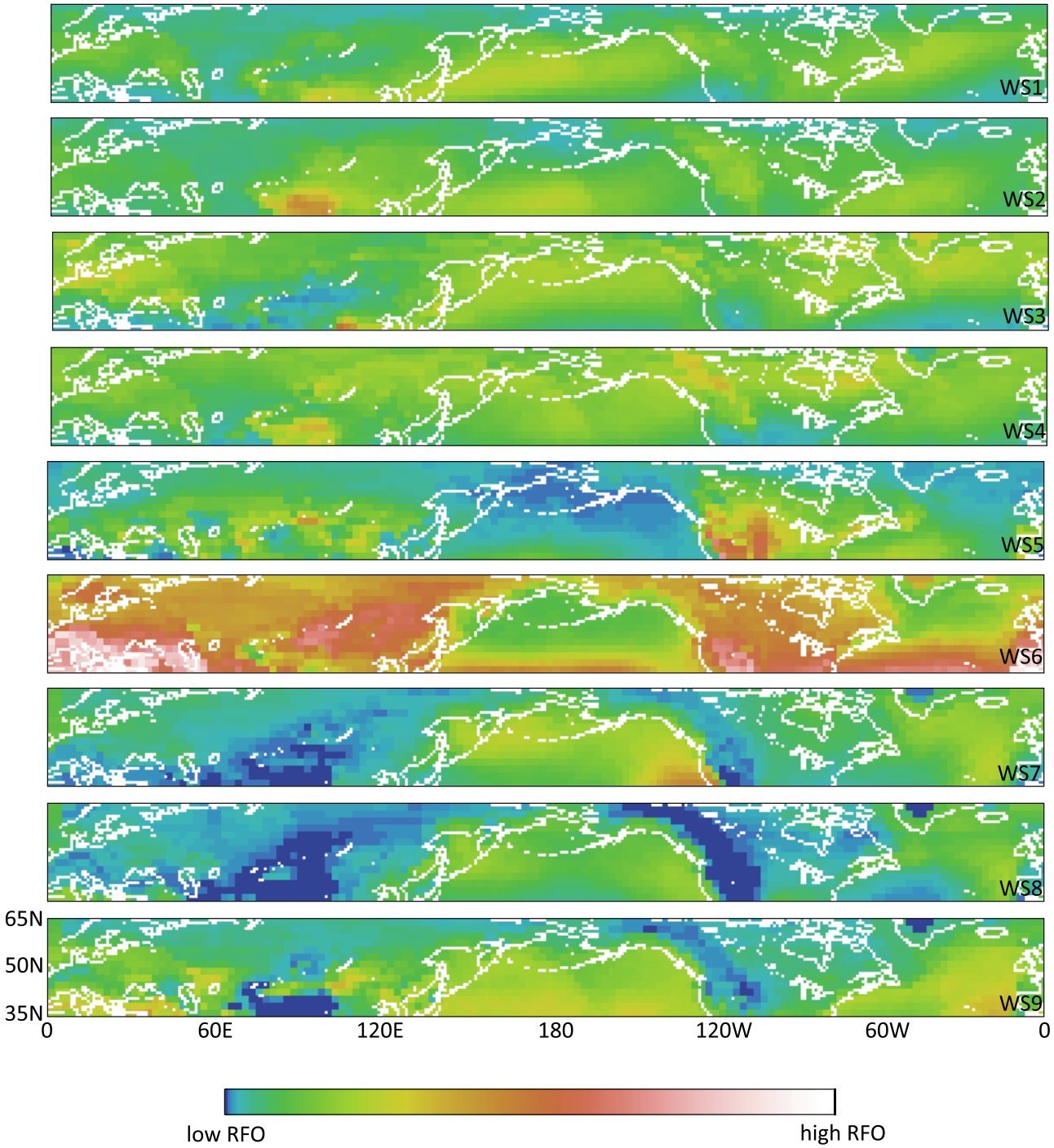

Figure 8. Same as Figure 2 but for the nine weather states of the northern midlatitudes.

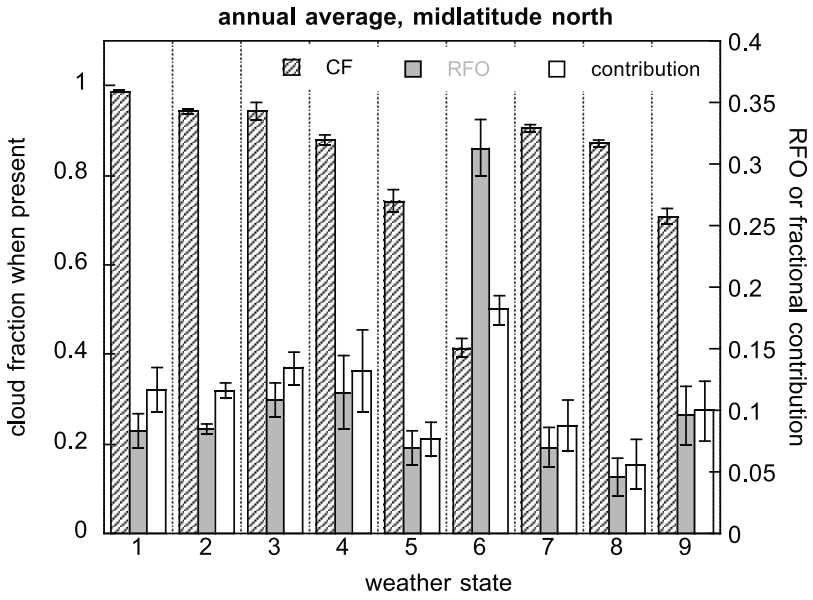

Figure 9. Same as Figure 3 but for the northern midlatitudes. The clear-sky (WS0) RFO is 0.014.

the largest seasonal variability in CF with a sdev approximately equal to 5% of the annual mean. WS5 and WS9 also have quite variable CFs, while WS1 (with a prevalence of deep frontal convection) on the other hand has the smallest sdev, with near overcast skies throughout the year. The mean CF is in general more seasonally variable than in the tropics (see Figure 3), but this is not true for all weather states (e.g., WS1 is one of these exceptions). The annual variation in RFO (indicated by the error bars superimposed on the mean RFOs of Figure 9) is, not surprisingly, more pronounced than that for the tropical weather states. WS4, WS5, WS7, WS8, and WS9 all have large annual cycles (sdev at least 20% of the annual mean) with WS8 (where stratus clouds are predominant) having perhaps the most dramatic RFO annual cycle, with July values ~67% above the annual mean and November values ~38% below (not shown). At the other end of the spectrum lies WS2 (with a predominance of cumulus congestus-like convective clouds) where the sdev of RFO is ~5% of the annual mean.

[22] The largest contributor (~18%) to total CF is WS6, the most frequent weather state, despite its low CF when present. The large contribution of WS6 is relatively steady from month to month (sdev equal to 6.5% of the annual mean). An even smaller annual cycle of contribution is exhibited by WS2 (a mixture of midlevel/high clouds of low τ). Five states (WS1, WS2, WS3, WS4, WS9) have 10% or above CF contributions. Of these, the most pronounced seasonal cycle of contribution is for WS4 (dominated by alto-type clouds) and WS9 (a multilayer mixture of boundary layer convection and high clouds), but their cycles are not in sync (not shown). The smallest contributor to midlatitude CF is WS8 (marine boundary layer cloud prevalence) despite its large cloud fraction when present; this is undoubtedly because it is the least frequent state.

[23] An important feature revealed by Figures 8 and 9 is that, while the distinctive land-concentrated WS6 is the most frequent state making the largest contribution to total CF in northern midlatitudes, the CF when present and RFO of all the other states are roughly equal with the "storm" types (WS1, WS2, WS3, WS4) having somewhat larger CF when present than the "fair weather" types (WS7, WS8, WS9). Another notable feature is that the first three states tend to separate in latitude, with WS1 demarking the classical storm tracks, WS2 shifted southward and WS3 shifted northward. WS4 is about evenly distributed over the whole storm track regime.

[24] The CRE behavior of northern midlatitude weather states is featured in Figures 10–12. A shallower troposphere and less intense convection yields a significantly weaker LW TOA CRE than in the tropics for the two most convectively active states, WS1 and WS2. The remaining seven states can be seen to belong to two groups of similar LW CRE, but generally distinct SW CRE. The first group (WS3, WS4, and WS5) has annual LW CRE ~35 Wm^{-2}, but SW mean CREs that differ by a factor of almost four; the second group (WS6, WS7, WS8, and WS9) has LW mean CREs ranging between 10 and 15 Wm^{-2} and a range of SW CREs nearly as wide as the previous group. The ordering of LW CRE strength follows almost exactly the ordering in terms of convection strength, but the strongest SW CREs come from weather states that can be very different in convective strength classification (WS1–WS7, WS3–WS8). WS1 and WS3, with large CFs when present and large τ, exhibit the largest mean SW CREs. WS2, i.e., the 2nd most convectively active state, has only the 5th largest SW CRE despite the fact that it also has the 2nd largest mean CF when present; this is likely because of the smaller τ that characterizes this regime compared to WS1 and WS3. The smallest mean SW CRE does not come from WS9 which has the lowest CF overall, but from WS6 which has smaller τ. It is notable that this most frequent state, has a nearly zero net daytime CRE. Seasonal variations of CRE are much more evident than in the tropics, especially for SW CRE which is affected by the annual cycle of available insolation. The

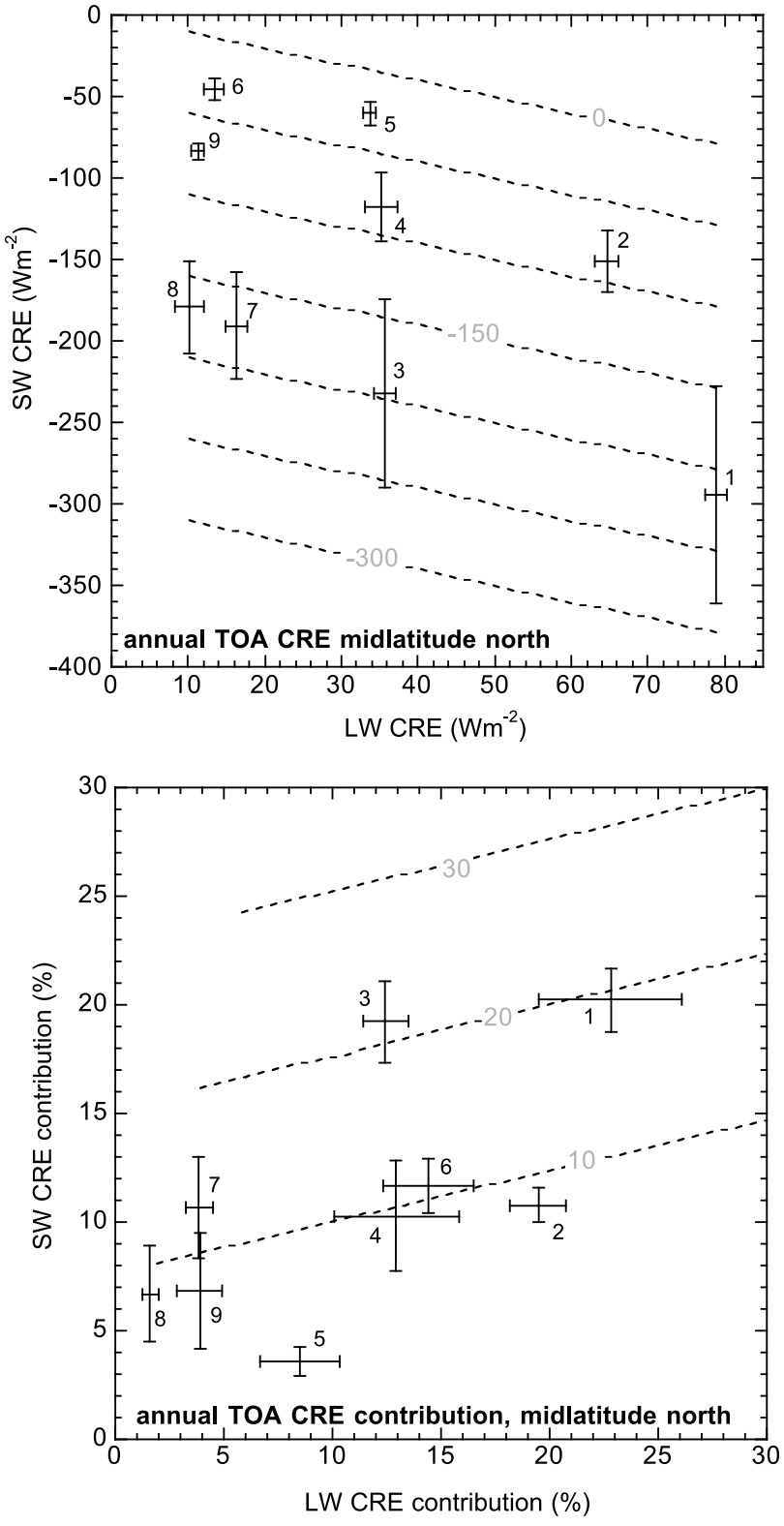

Figure 10. Same as Figure 4 but for the northern midlatitudes.

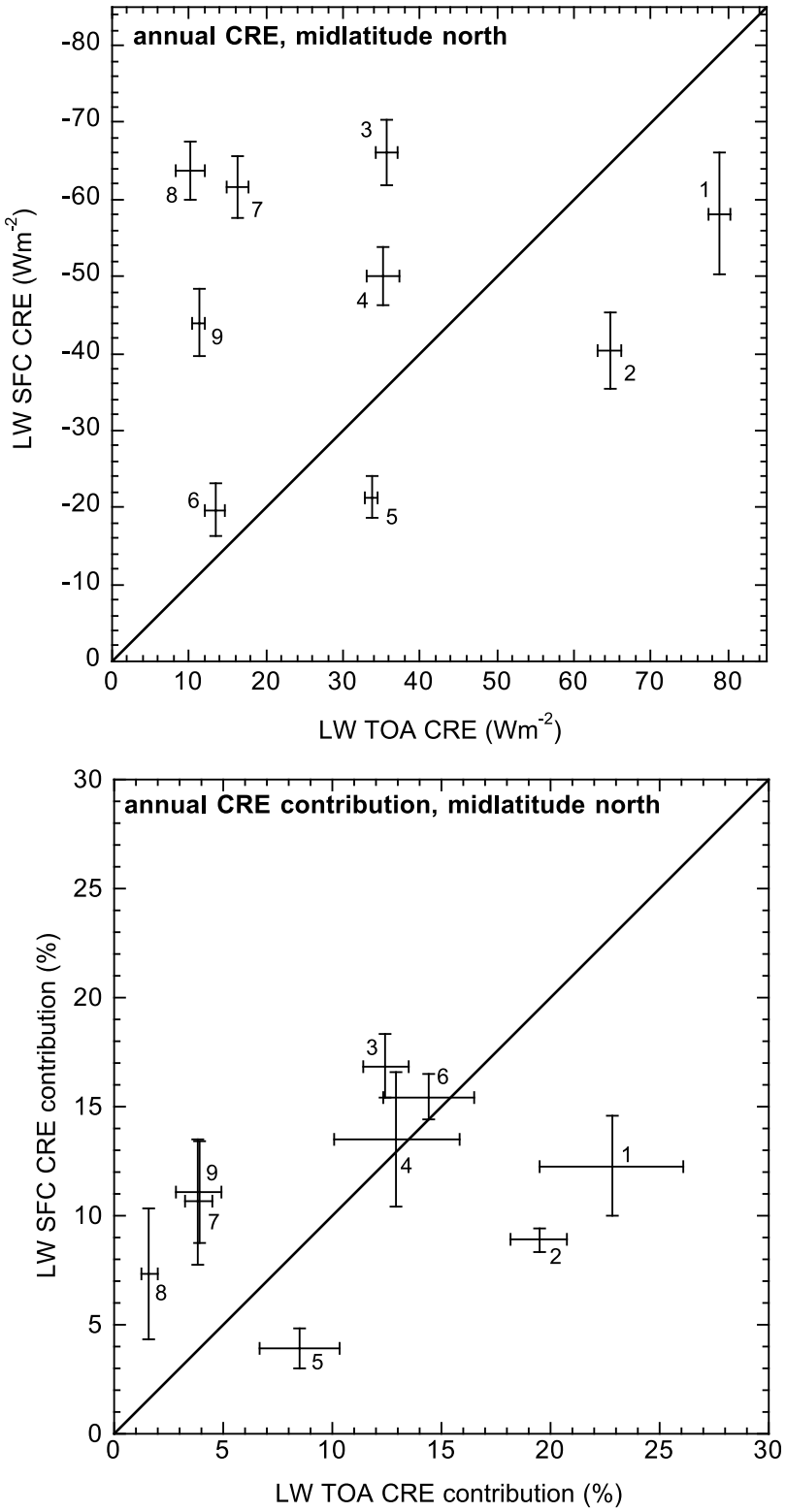

Figure 11. Same as Figure 5 but for the northern midlatitudes.

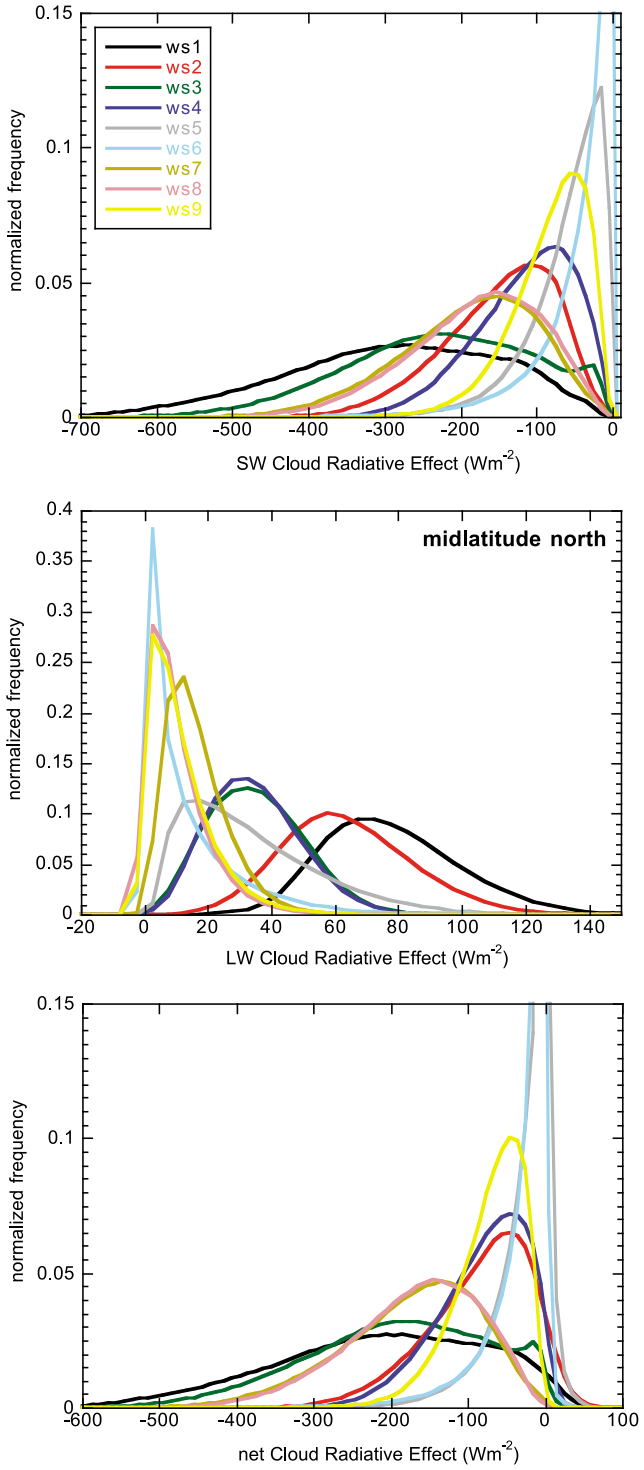

Figure 12. Same as Figure 6 but for the northern midlatitudes.

standard deviation of SW CRE reaches values as high as 25% of the mean (WS3), while all but one state have sdev greater than 10% of the mean. Even the LW CRE variability can occasionally be quite high in northern midlatitudes although it is still below 10% in general (the exception is WS8 at 19%).

[25] Figure 10 (bottom) indicates that WS1 and WS3 dominate the SW and net percent contributions to the northern midlatitude CRE total. WS1 has also the largest contribution to the LW CRE. Apparently the very high CF when present and generally higher cloud tops more than compensate for the third smallest RFO. Note that WS6 with small SW and LW mean CREs is a significant percent contributor presumably because it is the most frequent state in this geographical zone. Also note that three of the four states with smaller than 10% contribution to either the SW or LW CRE (WS5, WS7 and WS8) have the lowest RFOs. Both examples above serve as reminders of the role of RFO in CRE percent contributions and its irrelevance to mean CREs which are simple averages at the time of occurrence.

[26] Similarly to Figure 5, Figure 11 can be used to infer atmospheric LW CREs: the LW net flux magnitudes and percentage contributions are similar in showing that WS1 (chiefly frontal convection) and WS2 (chiefly the warm frontal stratiform component) produce significant atmospheric heating but also differ in that WS3 (with many nimbostratus in the cloud mixture) actually cools the atmosphere, reinforced by the fair weather states, except for WS5, which has much more cirrus and alto-type clouds. Thus, while fair weather low clouds produce atmospheric cooling, some parts of the storm clouds produce heating and some cooling.

[27] The histograms of the various components of CRE in Figure 12 reaffirm the similarity between WS1 and WS3 in SW and net CREs, but also highlight their difference in LW CRE (note that WS3 has a very similar histogram to WS4 in the LW). Even closer are the SW and net CRE histograms of WS7 and WS8, but this does not carry over to the LW, where WS8 mostly resembles WS9. The narrowest histograms for all CRE components correspond to WS6 (WS5 closely follows in the SW), and the widest for WS1, followed closely by WS3 (for SW and net CRE). Again, seasonal changes in insolation affect the SW and net CRE histograms, and tighter shapes would have been achieved had the seasonal cycle of incident solar radiation been removed.

4.3. Southern Midlatitudes

[28] The ISCCP weather state centroids for the southern midlatitudes are shown in Figure 13, while the geographic distribution of their frequency of occurrence is shown in Figure 14. Similar to Figures 3 and 9, Figure 15 shows the RFO, annually averaged CF when present, and contribution to the total CF of the zone. Both similarities and differences in CF characteristics compared to northern midlatitudes can be seen. Note that the southern hemisphere analysis is done independently of that for the northern hemisphere. The most remarkable aspect of these results is that the same weather states are found in both midlatitude zones (except for northern WS6 which is concentrated over land), supporting the contention that these cloud patterns are produced by the local (mesoscale) meteorological conditions.

[29] The fact that there is no counterpart to WS6 of the northern zone appears to be associated with the small amount of land present: northern WS5, which is similar to northern WS6 but with much less cirrus, shows concentrations over land that are also present in the southern zone, suggesting that the amounts of the counterpart southern weather state are too small to be separated in the analysis

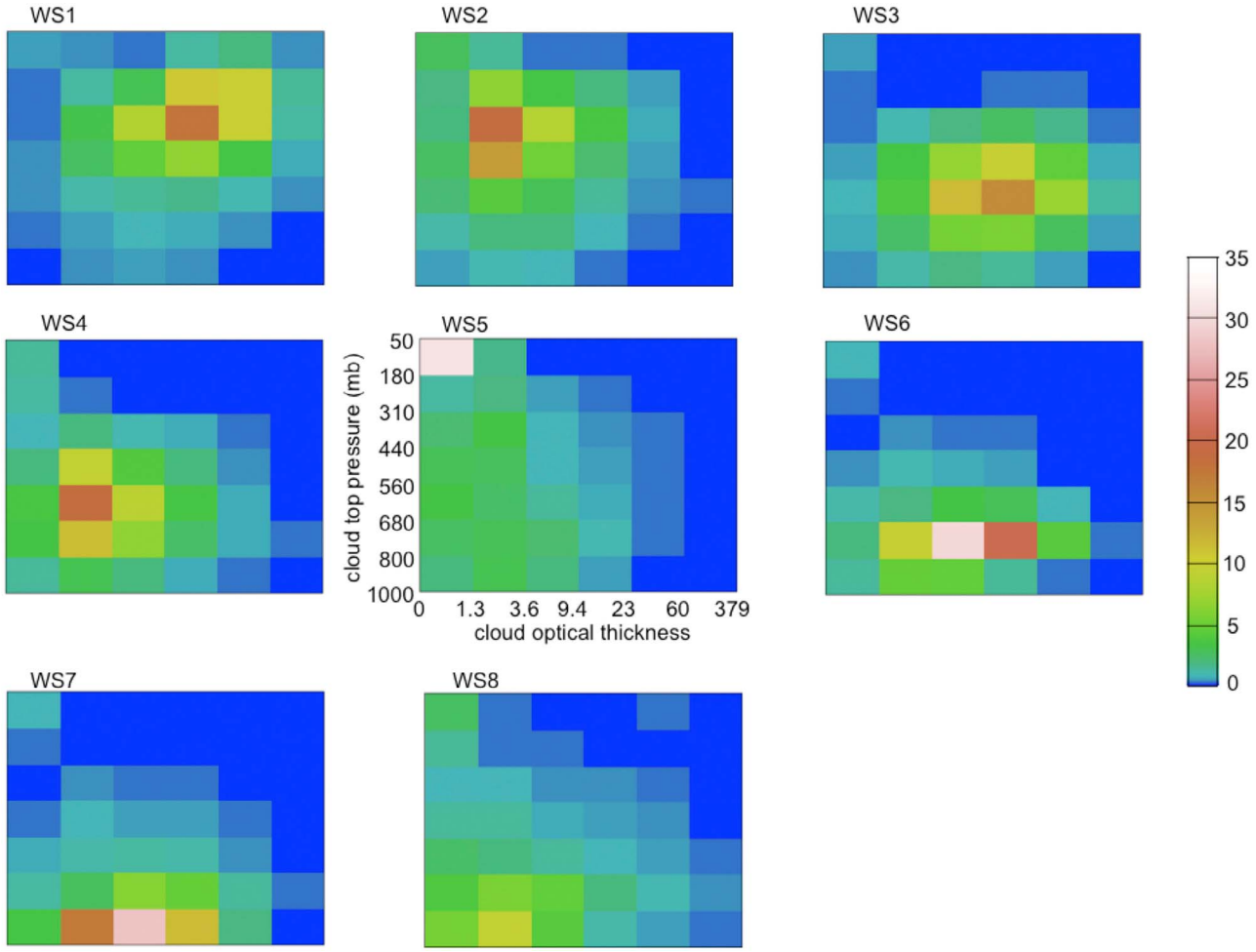

Figure 13. Same as Figure 1 but for the eight weather states of the southern midlatitudes (35°S to 65°S).

from southern WS5. Now the lowest mean CF when present (still always above 0.5) is encountered for WS8, a mixture of thin boundary layer clouds with some overlap by higher clouds. This state has the highest RFO and has also the most seasonally varying CF (albeit with a rather meager sdev equal to 3.5% of the mean). WS5 (where thin cirrus prevail) with mean CFs between 0.7 and 0.75 is between WS8 and all other weather states that form a group with mean CF above 0.85. WS8 is also the most seasonally varying with respect to its contribution to the total CF within the geographical zone; it almost doubles from summer to winter (not shown). WS8's top contribution to total CF reflects its far larger RFO compared to the other states. At the other extreme, the smallest contribution is by WS5 with the second smallest CF when present and lowest RFO. The annual change of RFO is not as dramatic for this geographical zone as in the north. Maximum deviations of ~42% and ~32% below and above the annual mean RFO (not shown) occur in June and November respectively for WS3 which contains relatively thick (optically and geometrically) frontal clouds (e.g., nimbostratus). The sdev of RFO is 25% of the mean for this weather state, which also has the largest annual cycle in CF contribution (sdev equal to 26% of the mean). The least variable state throughout the year in terms of CF, RFO and percent contribution is WS2 (containing the stratiform component of frontal convection) whose weak seasonal variability is similar to that of its northern WS2 counterpart.

[30] The CRE behavior of southern midlatitude weather states can be understood by examining Figures 16–18. As in the north, the annually and domain-averaged LW TOA CREs (Figure 16) are roughly ordered by strength of convective activity which largely determines the location of cloud tops, and the magnitudes of τ. In contrast, and similarly to what was shown before, the SW TOA CRE ordering does not follow the strength of convective activity. WS1 has greater LW CRE values than WS2 because of the greater τ of the highest clouds encountered in the former, but also because of the higher CF when present. For the same reasons it also has a larger SW CRE by ~150 Wm^{-2}. In general, the weather states appear quite well separated in LW-SW TOA CRE space and the separation generally carries over to the net TOA CRE with the exception perhaps of WS2 and WS4 which are otherwise easily distinguishable by their SW and LW CREs. The ordering of net CRE strength mirrors almost exactly the ordering of SW CRE strength. Changes in insolation cause some substantial seasonal variability (as indicated by the vertical error bars), which, in terms of ratio of sdev to mean, is

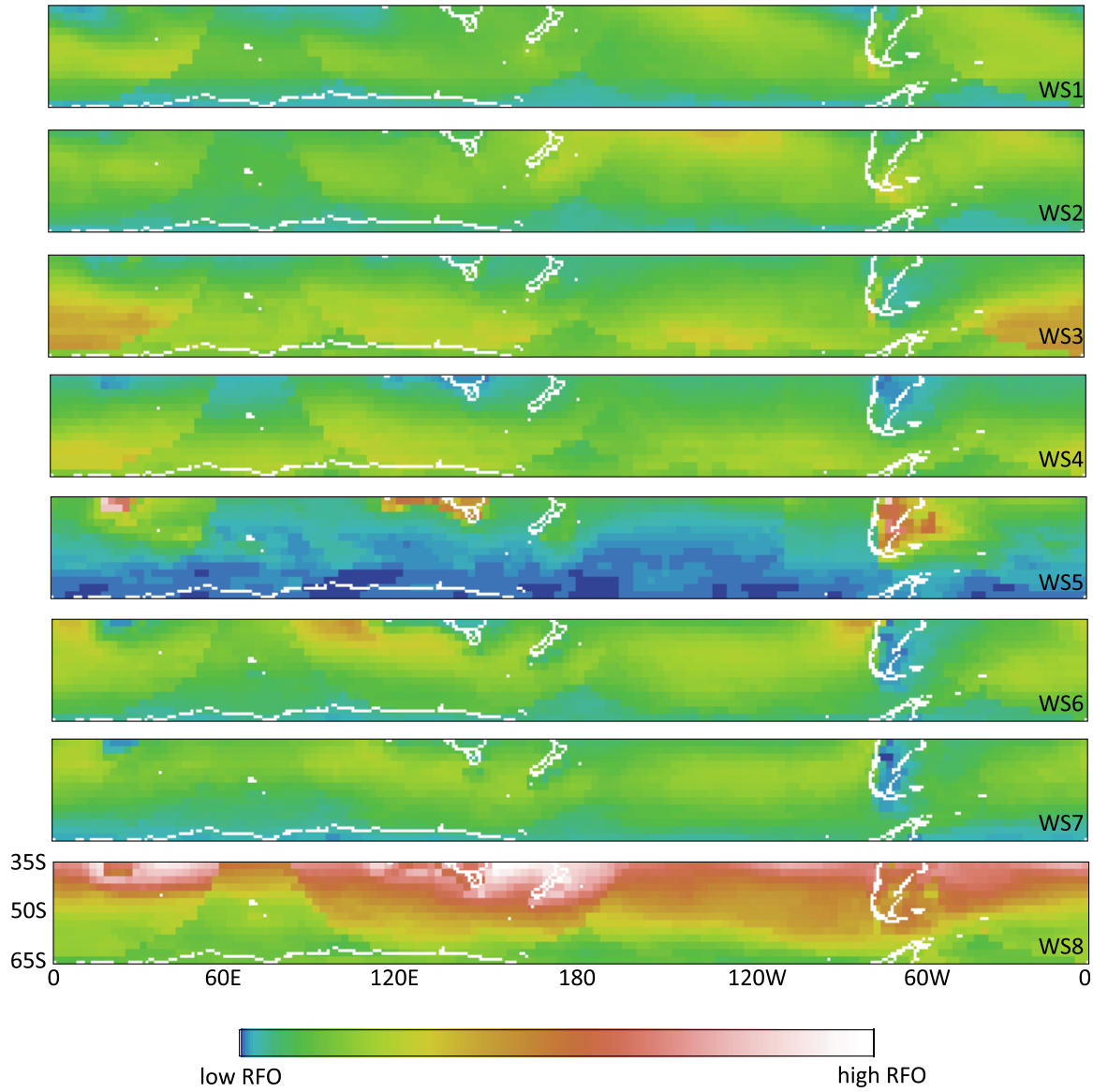

Figure 14. Same as Figure 2 but for the eight weather states of the southern midlatitudes.

close to 25% for four weather states (WS1, WS3, WS6 and WS7). Some of the larger variations occur for the weather states at higher latitudes (see Figure 14). LW CRE seasonal variability never exceeds 10%, but is still much larger than its counterpart in the tropics.

[31] The percent contribution to TOA CRE is shown in Figure 16 (bottom). While the domain-averaged LW CREs follow the ordering of convective strength, this is not the case for percent contributions. For example, the second weakest mean LW CRE of WS8 contributes significantly to the overall LW CRE because of this state's huge RFO of ~0.3. Contrast this with WS6 which provides a lower contribution because of its much lower RFO of ~0.11, despite the fact that the clouds it contains are colder than WS8 clouds,. The high RFO of WS8 is apparently sufficient to produce the third largest SW and net percent CRE contribution despite the state's low mean SW and net CRE. Overall, the largest SW and net CRE contribution come from WS3, the second most frequent state. Some of the big seasonal variabilities in SW CRE contribution (WS3 and WS8) have no analogs in the northern region. Figure 17 (the counterpart of Figures 5 and 11) implies that the LW CRE net in the atmosphere caused by the different states is qualitatively similar, but slightly weaker, than in the north. Also, notably weaker is seasonal variability in LW SFC CRE probably because of smaller contributions from atmospheric variability in the less extensive landmasses of the south.

[32] Notable features of the TOA CRE histograms (Figure 18) are again the large range of SW and net CRE values of WS1 and WS3, the surprising (given how different the cloud regimes they represent are) close resemblance of WS2 and WS7 SW CRE histograms (separation is achieved however in net CRE), and the similarity of WS3/WS4 and WS7/WS8 LW CRE histograms. In general, however, the

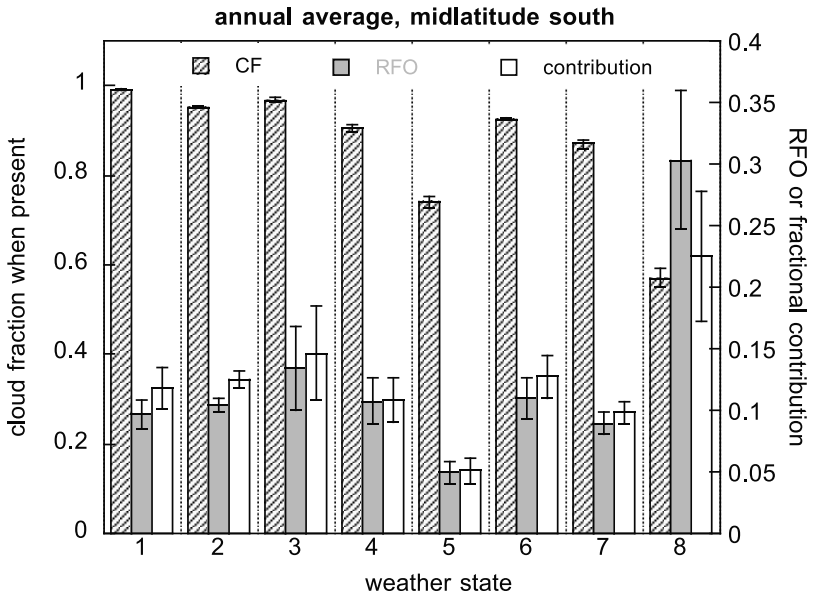

Figure 15. Same as Figure 3 but for the southern midlatitudes. The clear-sky (WS0) RFO is 0.0045.

CRE histograms indicate more radiatively distinct weather states in the southern than in the northern midlatitudes.

5. Discussion and Potential Applications

[33] Examining the ISCCP weather states found over most of the Earth's surface in the manner adopted in this study provides an opportunity to identify similarities and differences in their Cloud Radiative Effects (CREs) and to rank them not only on the basis of CRE magnitude at the time of occurrence, but also in terms of relative contributions to the total CRE which is greatly influenced their frequency of occurrence. In the tropics we found that the three most convectively active states are the ones with largest SW, LW and net TOA CRE contributions to the overall daytime tropical CRE budget. They account for 59%, 71% and 55% of the total CRE, respectively. The boundary layer–dominated weather states (WS5 to WS8) account for only 34% of the total SW CRE and 41% of the total net CRE, so to focus only on them in cloud feedback studies might not be wise, especially since these weather states occur predominantly in the subsidence part of the Hadley circulation that couples them to the convective weather states. In both the northern and southern midlatitude zones we revealed that only two weather states, the first and third most convectively active with large amounts of nimbostratus-type clouds, contribute ~40% to both the SW and net TOA CRE budgets, highlighting the fact that cloud regimes associated with frontal systems are not only important for weather (precipitation) but also for climate (radiation budget). While all cloud regimes in all geographical zones have a slightly larger SFC than TOA SW CRE (implying cooling of the surface and slight warming of the atmosphere), their LW radiative effects are more subtle. In the tropics the first four weather states with plentiful high clouds warm the atmosphere while the latter four with copious amounts of low clouds cool the atmosphere. In both midlatitude zones only the weather states with peak cloud fractions at levels above 440 mbar (WS1, WS2 and WS5 dominated by high clouds) warm the atmosphere while all the rest cool it. These are not entirely new insights but our results make the connection of the contrasting CRE effects to the atmospheric dynamics more explicit – "storms" tend to warm the atmosphere whereas fair weather cools it, suggesting a positive feedback of clouds on weather systems. With weather states being defined independently in the two midlatitude zones, it is interesting to discover both similarities (like the ones mentioned above) and differences, such as in the magnitudes of seasonal variability and the existence of an additional weather state in the northern zone occurring mostly over land. Despite the existence of this additional state only four weather states in the north have net CREs with absolute values above 100 Wm^{-2} compared to six in the south. This reminds us that the environment (primarily marine in the south) where clouds occur also has a crucial role in determining their radiative effects.

[34] Evaluations of the quality of present-day climate simulations by GCMs should not be based solely on large scale means, but must include the requirement that the correct radiation budget is produced for the right reasons. This makes correct simulation of the CRE contribution of individual weather states and of their association with specific meteorological situations in which they form of key importance. So, a first order validation test is to examine whether the cloud regimes produced by GCMs agree with those observed with regard to such properties as joint variations of cloud top pressure and optical thickness, frequency of occurrence, and cloud fraction. Such comparisons are possible now that most GCMs incorporate the ISCCP simulator as part of activities such as the Cloud Feedback Model Intercomparison Project (CFMIP, http://cfmip.metoffice.com/). The current study uses the ISCCP-based weather states to study their radiative effects. In doing so, we have created a data set that can be used in conjunction with the aforementioned ISCCP simulator to verify whether observed weather states can be reproduced by a GCM and that their associated CREs (means and contributions) are also correct.

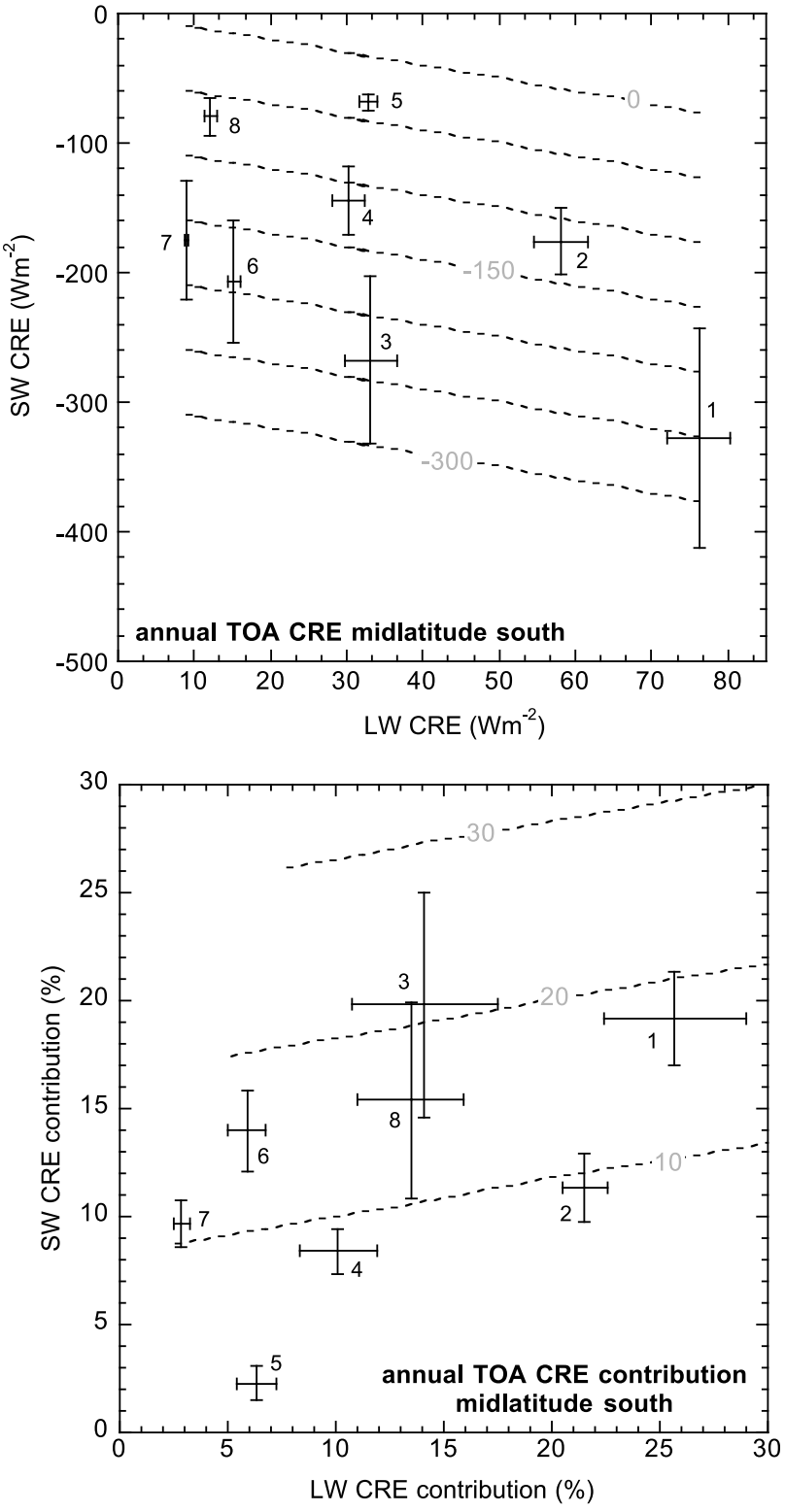

Figure 16. Same as Figure 4 but for the southern midlatitudes.

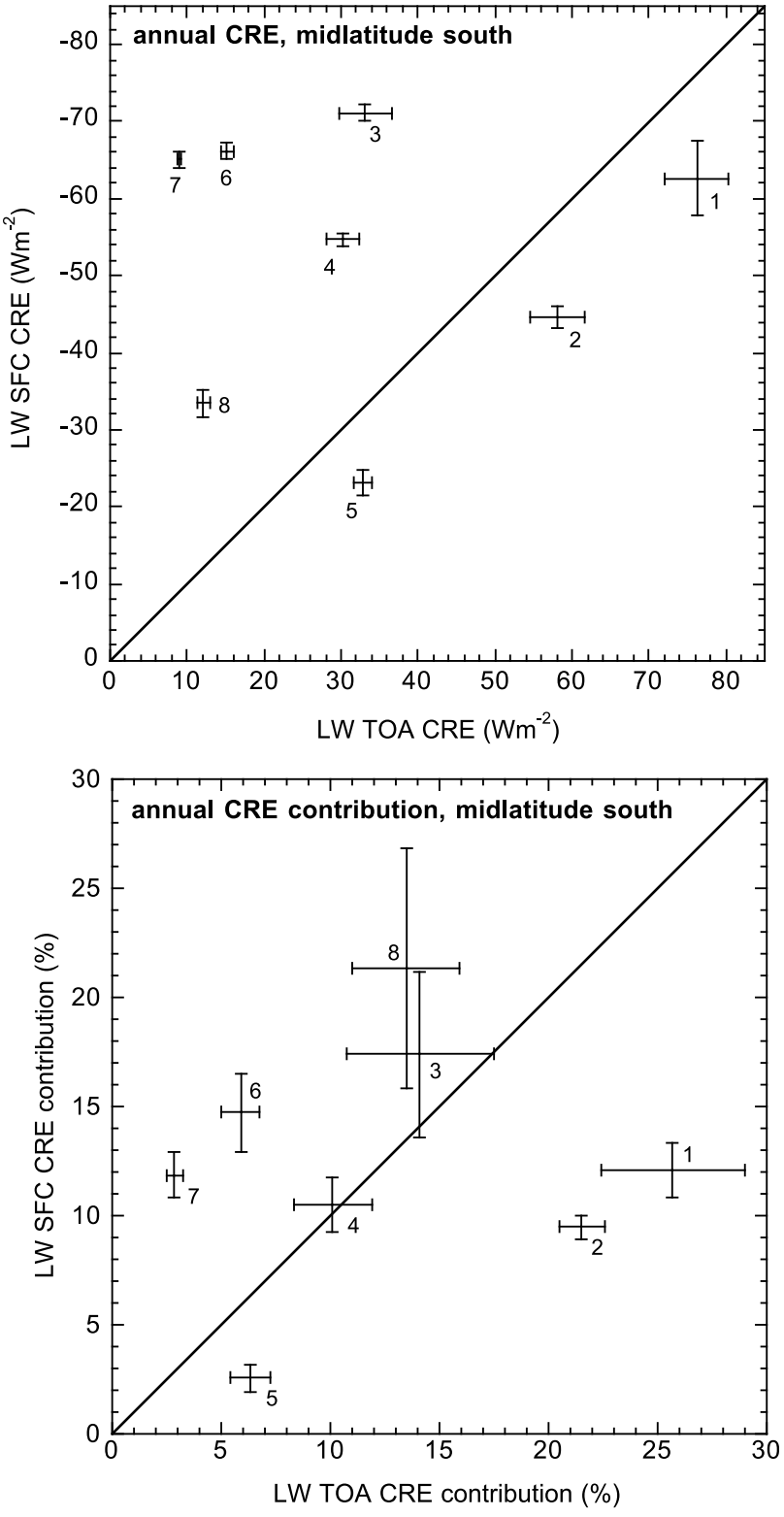

Figure 17. Same as Figure 5 but for the southern midlatitudes.

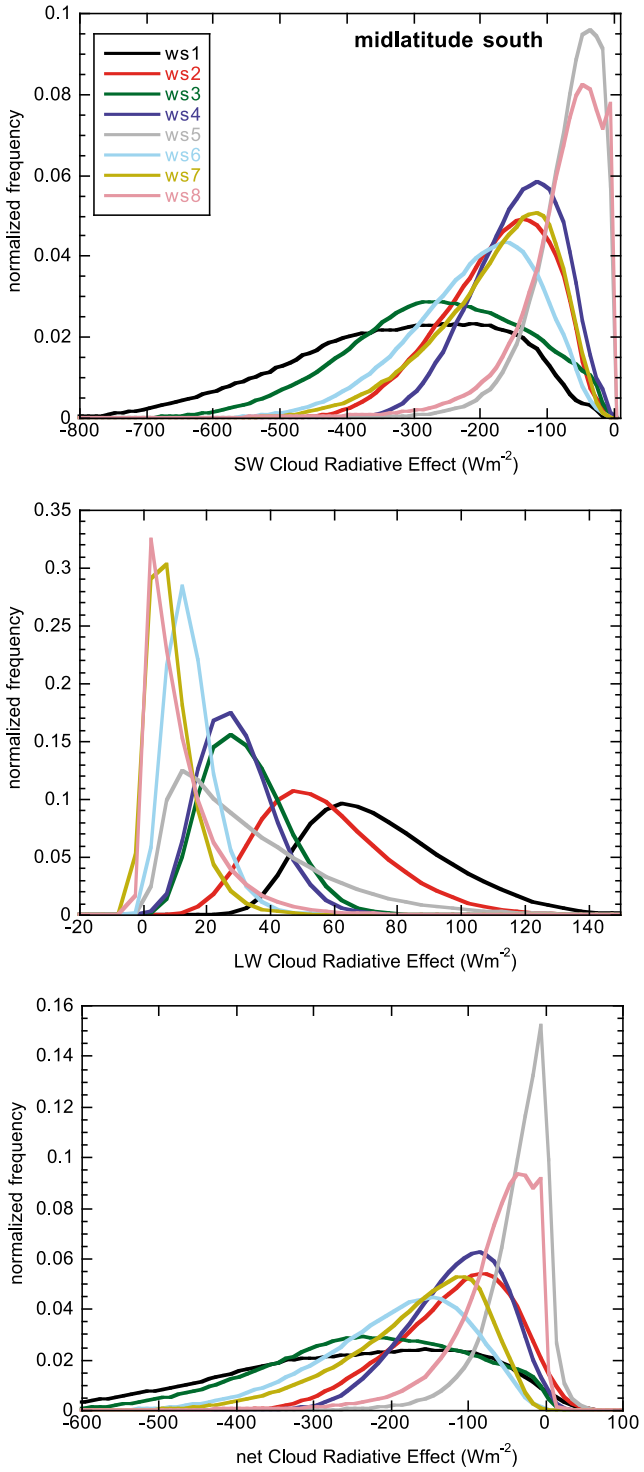

Figure 18. Same as Figure 6 but for the southern midlatitudes.

[35] Finally, we note that the results of our study provide support for the hypothesis that these cloud-property-based weather states provide a useful and distinctive classification in that they exhibit distinctive CRE values. Therefore, our results can also be used to adjust or fine tune the identification of centroids in a clustering analysis with data sets that are either similar to ISCCP (such as MODIS) or are based on entirely different observational principles (such as CloudSat/CALIPSO). This can be achieved by adding the constraint that the centroids are well separated not only in extinction-vertical location space, but also with respect to their CRE characteristics.

[36] **Acknowledgments.** Both authors acknowledge funding support under NASA's Modeling Analysis and Prediction (MAP) Program (grant NNXD7AN04G for W.B. Rossow) managed by David Considine.

References

Anderberg, M. R. (1973), *Cluster Analysis for Applications*, 359 pp., Academic, San Diego, Calif.

Chen, T., W. B. Rossow, and Y.-C. Zhang (2000), Radiative effects of cloud-type variations, *J. Clim.*, *13*, 264–286, doi:10.1175/1520-0442(2000)013<0264:REOCTV>2.0.CO;2.

Chen, Y., and A. D. Del Genio (2009), Evaluation of tropical cloud regimes in observations and a general circulation model, *Clim. Dyn.*, *32*, 355–369, doi:10.1007/s00382-008-0386-6.

Chéruy, F., and F. Aires (2009), Cluster analysis of cloud properties over the southern European Mediterranean area in observations and a model, *Mon. Weather Rev.*, *137*, 3161–3176, doi:10.1175/2009MWR2882.1.

Gordon, N. D., and J. R. Norris (2010), Cluster analysis of midlatitude oceanic cloud regimes: Mean properties and temperature sensitivity, *Atmos. Chem. Phys.*, *10*, 6435–6459, doi:10.5194/acp-10-6435-2010.

Gordon, N. D., J. R. Norris, C. P. Weaver, and S. A. Klein (2005), Cluster analysis of cloud regimes and characteristic dynamics of midlatitude synoptic systems in observations and a model, *J. Geophys. Res.*, *110*, D15S17, doi:10.1029/2004JD005027.

Greenwald, T. J., Y.-K. Lee, J. A. Otkin, and T. L'Ecuyer (2010), Evaluation of midlatitude clouds in a large-scale high-resolution simulation using CloudSat observations, *J. Geophys. Res.*, *115*, D19203, doi:10.1029/2009JD013552.

Hahn, C. J., W. B. Rossow, and S. G. Warren (2001), ISCCP cloud properties associated with standard cloud types identified in individual surface observations, *J. Clim.*, *14*, 11–28, doi:10.1175/1520-0442(2001)014<0011:ICPAWS>2.0.CO;2.

Hartmann, D. L., M. E. Ockert-Bell, and M. L. Michelsen (1992), The effect of cloud type on Earth's energy balance: Global analysis, *J. Clim.*, *5*, 1281–1304, doi:10.1175/1520-0442(1992)005<1281:TEOCTO>2.0.CO;2.

Haynes, J. M., C. Jakob, W. B. Rossow, G. Tselioudis, and J. Brown (2011), Major characteristics of southern ocean cloud regimes and their effects on the energy budget, *J. Clim.*, doi:10.1175/2011JCLI4052.1.

Jakob, C., and G. Tselioudis (2003), Objective identification of cloud regimes in the tropical western Pacific, *Geophys. Res. Lett.*, *30*(21), 2082, doi:10.1029/2003GL018367.

Jakob, C., G. Tselioudis, and T. Hume (2005), The radiative, cloud and thermodynamic properties of the major tropical western Pacific cloud regimes, *J. Clim.*, *18*, 1203–1215, doi:10.1175/JCLI3326.1.

Klein, S. A., and D. L. Hartmann (1993), The seasonal cycle of low stratiform clouds, *J. Clim.*, *6*, 1587–1606, doi:10.1175/1520-0442(1993)006<1587:TSCOLS>2.0.CO;2.

Klein, S. A., and C. Jakob (1999), Validation and sensitivities of frontal clouds simulated by the ECMWF model, *Mon. Weather Rev.*, *127*, 2514–2531, doi:10.1175/1520-0493(1999)127<2514:VASOFC>2.0.CO;2.

Lau, N.-C., and M. W. Crane (1995), A satellite view of the synoptic-scale organization of cloud properties in midlatitude and tropical circulation systems, *Mon. Weather Rev.*, *123*, 1984–2006, doi:10.1175/1520-0493(1995)123<1984:ASVOTS>2.0.CO;2.

Marchand, R., N. Beagley, and T. P. Ackerman (2009), Evaluation of hydrometeor occurrence profiles in the multiscale modeling framework climate model using atmospheric classification, *J. Clim.*, *22*, 4557–4573, doi:10.1175/2009JCLI2638.1.

Mekonnen, A., and W. B. Rossow (2011), The interaction between deep convection and easterly waves tropical North Africa: A weather state perspective, *J. Clim.*, doi:10.1175/2011JCLI3900.1, in press.

Oreopoulos, L., and R. Davies (1993), Statistical dependence of albedo and cloud cover on sea surface temperature for two tropical marine stratocumulus regions, *J. Clim.*, *6*, 2434–2447, doi:10.1175/1520-0442(1993)006<2434:SDOAAC>2.0.CO;2.

Pincus, R., C. P. Batstone, R. J. P. Hofmann, K. E. Taylor, and P. J. Glecker (2008), Evaluating the present-day simulation of clouds, precipitation, and radiation in climate models, *J. Geophys. Res.*, *113*, D14209, doi:10.1029/2007JD009334.

Ramanathan, V., E. Ahmad, R. D. Cess, E. F. Harrison, P. Minnis, B. R. Barkstrom, and D. Hartmann (1989), Cloud-radiative forcing and climate: Results from the Earth Radiation Budget Experiment, *Science*, *243*, 57–63, doi:10.1126/science.243.4887.57.

Rossow, W. B., and A. A. Lacis (1990), Global, seasonal cloud variations from satellite radiance measurements. Part II: Cloud properties and radiative effects, *J. Clim.*, *3*, 1204–1253, doi:10.1175/1520-0442(1990)003<1204:GSCVFS>2.0.CO;2.

Rossow, W. B., and R. A. Schiffer (1991), ISCCP cloud data products, *Bull. Am. Meteorol. Soc.*, *72*, 2–20, doi:10.1175/1520-0477(1991)072<0002:ICDP>2.0.CO;2.

Rossow, W. B., and R. A. Schiffer (1999), Advances in understanding clouds from ISCCP, *Bull. Am. Meteorol. Soc.*, *80*, 2261–2287, doi:10.1175/1520-0477(1999)080<2261:AIUCFI>2.0.CO;2.

Rossow, W. B., and Y.-C. Zhang (1995), Calculation of surface and top-of-atmosphere radiative fluxes from physical quantities based on ISCCP datasets: 2. Validation and first results, *J. Geophys. Res.*, *100*, 1167–1197, doi:10.1029/94JD02746.

Rossow, W. B., G. Tselioudis, A. Polak, and C. Jakob (2005), Tropical climate described as a distribution of weather states indicated by distinct mesoscale cloud property mixtures, *Geophys. Res. Lett.*, *32*, L21812, doi:10.1029/2005GL024584.

Schiffer, R. A., and W. B. Rossow (1983), The International Satellite Cloud Climatology Project (ISCCP): The first project of the World Climate Research Programme, *Bull. Am. Meteorol. Soc.*, *64*, 779–784.

Tromeur, E., and W. B. Rossow (2010), Interaction of tropical deep convection with the large-scale circulation in the Madden-Julian oscillation, *J. Clim.*, *23*, 1837–1853, doi:10.1175/2009JCLI3240.1.

Tselioudis, G., and W. B. Rossow (2011), Time scales of variability of the tropical atmosphere derived from cloud-defined weather states, *J. Clim.*, *24*, 602–608, doi:10.1175/2010JCLI3574.1.

Warren, S. G., C. J. Hahn, J. London, R. M. Chervin, and R. L. Jenne (1986), Global distribution of total cloud cover and cloud type amounts over land, *Tech. Rep. TN-273 1 STR*, 29 pp., Natl. Cent. for Atmos. Res., Boulder, Colo.

Warren, S. G., C. J. Hahn, J. London, R. M. Chervin, and R. L. Jenne (1988), Global distribution of total cloud cover and cloud type amounts over the ocean, *Tech. Rep. TN-317 1 STR*, 42 pp., Natl. Cent. for Atmos. Res., Boulder, Colo.

Webb, M., C. Senior, S. Bony, and J.-J. Morcrette (2001), Combining ERBE and ISCCP data to assess clouds in the Hadley Centre, ECMWF and LMD atmospheric climate models, *Clim. Dyn.*, *17*, 905–922, doi:10.1007/s003820100157.

Williams, K. D., and G. Tselioudis (2007), GCM intercomparison of global cloud regimes: Present-day evaluation and climate change response, *Clim. Dyn.*, *29*, 231–250, doi:10.1007/s00382-007-0232-2.

Williams, K. D., and M. J. Webb (2009), A quantitative performance assessment of cloud regimes in climate models, *Clim. Dyn.*, *33*, 141–157, doi:10.1007/s00382-008-0443-1.

Zhang, Y.-C., W. B. Rossow, and A. A. Lacis (1995), Calculation of surface and top-of-atmosphere radiative fluxes from physical quantities based on ISCCP datasets: 1. Method and sensitivity to input data uncertainties, *J. Geophys. Res.*, *100*, 1149–1165, doi:10.1029/94JD02747.

Zhang, Y., W. B. Rossow, A. A. Lacis, V. Oinas, and M. I. Mishchenko (2004), Calculation of radiative fluxes from the surface to top of atmosphere based on ISCCP and other global data sets: Refinements of the radiative transfer model and the input data, *J. Geophys. Res.*, *109*, D19105, doi:10.1029/2003JD004457.

Zhang, Y., S. Klein, G. G. Mace, and J. Boyle (2007), Cluster analysis of tropical clouds using CloudSat data, *Geophys. Res. Lett.*, *34*, L12813, doi:10.1029/2007GL029336.

Zhang, Y., S. Klein, J. Boyle, and G. G. Mace (2010), Evaluation of tropical cloud and precipitation statistics of Community Atmosphere Model version 3 using CloudSat and CALIPSO data, *J. Geophys. Res.*, *115*, D12205, doi:10.1029/2009JD012006.

L. Oreopoulos, Laboratory for Atmospheres, NASA Goddard Space Flight Center, Code 613.2, Greenbelt, MD 20771, USA. (lazaros.oreopoulos@nasa.gov)

W. B. Rossow, NOAA Cooperative Remote Sensing Science and Technology Center, City College of New York, 160 Convent Ave., New York, NY 10031, USA.